Journal of Russian Laser Research, Volume 25, Number 6, 2004

INELASTIC LIGHT SCATTERING NEAR THE FERROELECTRIC PHASE-TRANSITION POINT IN BISMUTH VANADATE CRYSTALS

L. P. Avakyants,[1] A. V. Chervyakov,[2] V. S. Gorelik,[2] and P. P. Sverbil'[2]

[1] *Physics Department, M. V. Lomonosov Moscow State University*
Vorobievy Gory, Moscow 119899, Russia
[2] *P. N. Lebedev Physical Institute, Russian Academy of Sciences*
Leninskii Pr. 53, Moscow 119991, Russia
e-mail: gorelik@sci.lebedev.ru

Abstract

The Raman and Brillouin spectra in bismuth vanadate crystals near the ferroelectric phase-transition point are studied. The intensity maximum corresponding to the soft mode in light scattering spectra is found. This mode is responsible for the instability of the bismuth vanadate crystal lattice in the vicinity of the ferroelectric phase-transition point. Strong interaction of the soft optical mode with an acoustic mode of the corresponding symmetry is revealed by an analysis of the Raman and Brillouin spectra observed. The theory of light scattering by coupled lattice modes based on the model of two strongly coupled oscillators is developed. The introduction of an additional oscillator strongly interacting with the fundamental soft mode is shown to result in a temperature shift of the structural phase transition to higher temperatures. The results obtained confirm the possibility of changing the phase-transition temperature by modification of the vibrational spectrum through introduction of additional degrees of freedom or comminution of the macroscopic sample with formation of the ordered superdispersed structure (globular crystal). These results are general and can be subsequently used to increase the phase-transition temperature in ferroelastics, ferroelectrics, and superconductors.

Keywords: Raman scattering, Brillouin scattering, structural phase transition, soft mode, crystal lattice.

1. Introduction

Modern achievements in optoelectronics, acoustics, and acousto-optics rely on the use of new synthetic single crystals. These materials exhibit electrooptic, piezooptic, and acoustooptic properties important for applications. Along with the ferroelectric crystals $LiNbO_3$, $KH_2(PO_4)$ (KDP), $LiTaO_3$, and so on that are customarily used, the new ferroelastic materials (TeO_2, Hg_2Cl_2, $BiVO_4$, $Pb_3(VO_4)_2$, and so on) are of significant promise for applications. These new materials are characterized by anomalously high refractive indexes and small sound velocities. Thus, they possess improved acoustooptic efficiency and ferroelectric properties.

Studies of the ferroelastic phase transition in these materials are of both fundamental (associated with the study of the general mechanisms of structural phase transitions) and applied importance. The latter consists in the prospects of using the high lattice lability arising in the phase-transition region for creation of new highly sensitive technical tools and devices. In this case, the thermal stability of parameters of

Translated from a manuscript submitted July 13, 2004.
1071-2836/04/2506-0535

the specific devices operating at temperatures far from the phase-transition region is defined in many ways by the nature and magnitude of the anomalies in physical properties in the phase-transition region.

According to the modern theory of structural phase transitions in condensed matter, the dielectric, elastic, and elasto-optical anomalies of crystals are due to the lattice instability with respect to the specific vibration. This vibration is called a soft mode and strongly interacts with other modes. The interaction of the soft mode with other lattice vibrations can be studied by an analysis of the spectra of IR absorption, Raman scattering, and Brillouin scattering.

Such an interaction results in renormalization of the thermodynamic characteristics of the phase transition. This provides the possibility of variation of the phase-transition temperature at the expense of changing the parameters of low-frequency lattice vibrations by the introduction of impurities, intercalation, and so on.

It should be noted that the relation of the vibrational spectra of crystals to their elastic and optical properties was previously studied mainly for ferroelectrics. One should expect similar results for ferroelastic crystals without the piezoelectric effect but with the symmetry-allowed linear interaction of the order parameter and deformation.

In this connection, this paper studies the problem of the vibrational spectra of ferroelastic crystals of bismuth vanadate ($BiVO_4$). These crystals undergo ferroelastic phase transitions of the second kind at $T_c = 522$ K and possess high acousto-optical efficiency, small sound damping, and good optical quality. Because of these characteristics, bismuth vanadate shows promise for acousto-optics.

However, practical implementation of this material was hampered by the lack of data on the refractive indexes and elastic moduli and their temperature dependences. In addition, lack of these data hampers a correlation between the results of the experiment and phase-transition theory for bismuth vanadate.

The main goal of the present paper is to study the specific features of light scattering by the acoustic and optical modes of $BiVO_4$ ferroelastic crystals under the condition of strong coupling between these modes in a temperature range that includes the phase-transition point ($T_c = 522$ K).

2. Theory of Light Scattering in the Region of the Ferroelastic Phase Transition

2.1. Theory of Light Scattering by Lattice Vibrations in the Case of Coupling Between Oscillators

Studies of phase transitions in detail were started by Ginzburg and Levanyuk [1–3] and Cochran [4]. In these papers, the specific features of light scattering by the so-called soft modes near the phase-transition points of the second kind were indicated.

As is well known [5, 6] the condition of stability of the crystal lattice is the reality and distinction from zero of all characteristic frequencies ω defined by the secular equation

$$|\Phi_{ij}^{\mu\nu} - m_\mu \omega^2 \delta_{\mu\nu} \delta_{ik}| = 0. \tag{2.1}$$

Here, Φ is the force-constant matrix, m is the mass, and δ is the Kronecker symbol.

The condition of existence of only positive solutions is fulfilled when all principal minors of the determinant of the matrix Φ are positive, i.e.,

$$\det|\Phi| > 0. \tag{2.2}$$

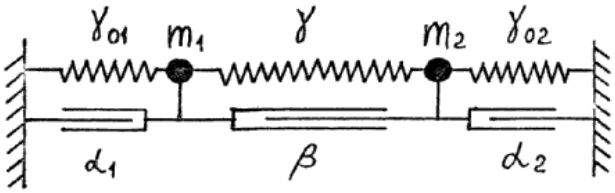

Fig. 1. System of two coupled oscillators.

It is apparent that one should not restrict oneself to the purely harmonic approximation in the original equations to obtain the temperature dependences of the parameters entering the matrix Φ. These dependences result in the violation of condition (2.2) at a certain temperature. However, even a small anharmonicity entering into these equations causes a considerable complication of the whole problem. In this case, it is appropriate to seek a violation of condition (2.2) for some individual (soft) modes [7] that determine the change in the crystal symmetry and to account for the anharmonicity of other modes through their coupling with the soft modes. In these conditions the mean value of the normal coordinate of the soft mode can serve as an order parameter. One can also try to consider the dielectric, elastic, and elasto-optical anomalies from the unified point of view in terms of the lattice stability.

The results of coupling of the lattice vibrational modes manifest themselves clearly in the spectra of IR absorption and Raman and Brillouin scattering in the form of the characteristic "repulsion" of lines and redistribution ("transfer") of intensity from one mode to another [8, 9]. The specific features of Raman scattering by the bound vibrational states in ferroelectric crystals were studied in detail by Gorelik [8,10]. The extensive literature dedicated to the soft ferroelectric modes can be found in reviews [8–11].

To better understand the essence of the processes occurring on interaction of the soft mode with other fundamental vibrations, we turn our attention to the idealized model of two coupled oscillators considered in [8] (see Fig. 1). The equations of motion of such a system have the form

$$m_1\ddot{u}_1 = -\gamma - \gamma(u_1 - u_2) - \alpha_1\dot{u}_1 - \beta(\dot{u}_1 - \dot{u}_2), \tag{2.3}$$

$$m_2\ddot{u}_2 = -\gamma_{02}u_2 - \gamma(u_2 - u_1) - \alpha_2\dot{u}_2 - \beta(\dot{u}_2 - \dot{u}_1). \tag{2.4}$$

Using the Green's function formalism the author of [8] showed the possibility of existence of two normal modes in a system with frequencies

$$\Omega_\pm^2 = \frac{1}{2}(\Omega_1^2 + \Omega_2^2) \pm \frac{1}{2}\sqrt{(\Omega_1^2 - \Omega_2^2) + 4\Delta_{12}^2\Delta_{21}^2}\,, \tag{2.5}$$

where

$$\Omega_1^2 = \frac{\gamma_{01} + \gamma}{m_1}\,, \quad \Omega_2^2 = \frac{\gamma_{02} + \gamma}{m_2}\,, \quad \Delta_{12}^2 = \frac{\gamma}{m_1}\,, \quad \Delta_{21}^2 = \frac{\gamma}{m_2}\,.$$

The spectral distribution of inelastically scattered radiation for a system of such type has the form

$$I(\Omega) = \left(\frac{\partial\alpha}{\partial u}\right)^2 \chi''(\Omega)|m(\Omega) + 1|. \tag{2.6}$$

Here, $\partial\alpha/\partial u$ is the derivative of polarizability with respect to the normal coordinate, which characterizes the Raman intensity, $[m(\Omega) + 1]$ is the Bose–Einstein factor, and $\chi''(\Omega)$ is the imaginary part of the

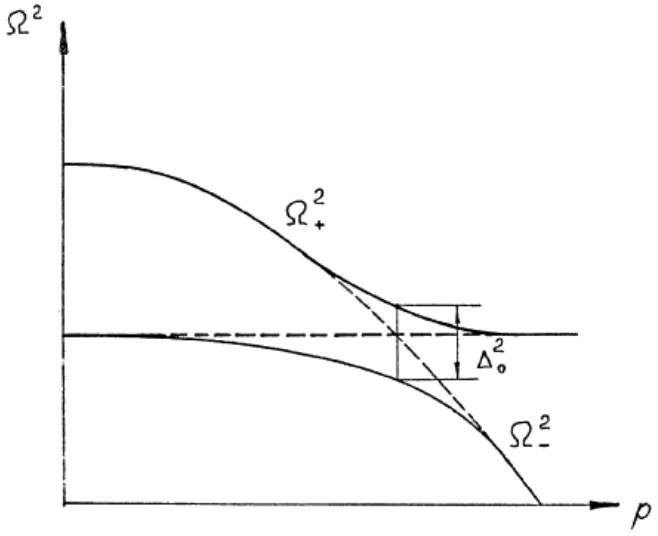

Fig. 2. The effect of "frequency repulsion" in the interaction of two oscillators.

susceptibility

$$\chi(\Omega) = \sum_{i,j=1,2} p_i p_j G_{ij}(\Omega). \tag{2.7}$$

The coefficients p_i and p_j characterize the contribution of each oscillator to the Raman intensity and $G_{ij}(\Omega)$ is the Green's function,

$$||G_{ij}^{-1}|| = \left\| \begin{matrix} (\Omega^2 - \Omega_1^2 + i\Gamma_1\Omega) & (\Delta_{12}^2 + i\Gamma_{12}\Omega) \\ (\Delta_{21}^2 + i\Gamma_{21}\Omega) & (\Omega^2 - \Omega_2^2 + i\Gamma_2\Omega) \end{matrix} \right\|, \tag{2.8}$$

$$\Gamma_1 = \frac{\alpha_1 + \beta}{m_1}\,, \quad \Gamma_2 = \frac{\alpha_2 + \beta}{m_2}\,, \quad \Gamma_{12} = -\frac{\beta}{m_1}\,, \quad \Gamma_{21} = -\frac{\beta}{m_2}\,.$$

The separation between the frequencies of the interacting oscillators is determined by the relationship

$$\Omega_+^2 + \Omega_-^2 = \sqrt{(\Omega_1^2 - \Omega_2^2)^2 = 4\Delta_{12}^2\Delta_{21}^2}\,. \tag{2.9}$$

When the partial frequency of one of the coupled oscillators strongly varies with some external factor (temperature, pressure, and so on), i.e., $\gamma_{01}/m_1 = f(p)$, while the corresponding frequency of the other oscillator remains constant, $\gamma_{02}/m_2 = \text{const}$ (such a case can be realized near the phase-transition point in a crystal), the strong interaction of modes sets in under certain conditions. This interaction is accompanied by drastic frequency tuning according to (2.5). With the equality of the frequencies ($\Omega_1 = \Omega_2$) their "repulsion" occurs by the value

$$\Delta_0 = \sqrt{2\Delta_{12}\Delta_{21}} = \gamma\sqrt{2/m_1 m_2}\,. \tag{2.10}$$

The variations in the spectrum caused by this interaction are shown in Fig. 2.

The characteristics of the phase transition change with switching on of the interaction of the soft mode with some additional low-frequency vibration. Let us assume that the partial frequency of one of

the modes is $\Omega_{01}^2 = \gamma_{01}/m_1 = a(\theta - T)$, while that of another mode is $\Omega_{02}^2 = \gamma_{02}/m_2 = \text{const}$ ($\Omega_{02}^2 < \Omega_{01}^2$, θ is the transition temperature). Using expressions (2.5) we obtain the following relationship for the renormalized frequency of the soft mode:

$$\Omega_-^2 = a'(\theta' - T) = \frac{1}{2}\left[a(\theta - T) + \frac{\gamma}{m_1} + \Omega_2^2\right] - \frac{1}{2}\sqrt{\left[a(\theta - T) + \frac{\gamma}{m_1} - \Omega_2^2\right]^2 + \frac{4\gamma^2}{m_1 m_2}}\,. \tag{2.11}$$

In this case, the expressions for the parameters a' and θ' have the form

$$a' = a\frac{m_1(\gamma_0 2 + \gamma)}{2\gamma\gamma_{02}}\left[\left(\frac{\gamma}{m_1} + \frac{\gamma_{02} + \gamma}{m_2}\right) - \sqrt{\left(\frac{\gamma_{02} + \gamma}{m_2} - \frac{\gamma}{m_1}\right)^2 + \frac{4\gamma^2}{m_1 m_2}}\right], \tag{2.12}$$

$$\theta' = \theta + \frac{1}{a}\cdot\frac{\gamma\gamma_{02}}{m_1(\gamma_{02} + \gamma)}\,. \tag{2.13}$$

From relationships (2.12) and (2.13), one sees how the characteristics of the phase transition are renormalized because of the interaction of the soft mode with the low-frequency crystal modes and how one can "control" these characteristics. In particular, with interaction between the soft and deformation modes, a phase transition always takes place at the temperature T_c, which exceeds the temperature T_0 of the phase transition of the system without interaction [12,13]. This allows one to vary the phase-transition temperature T_0 at the expense of change in the parameters of the low-frequency crystal vibrations, by doping, intercalation, comminution, and other external actions [8].

It is important that the effects discussed should take place not only for the structural phase transitions (in particular, for the ferroelectric and ferroelastic ones) but also for the other phase transitions characterized by the presence of the soft mode, i.e., described by a theory of the Ginzburg–Landau type. Of particular interest from this point of view is the possibility of enhancing the temperature of the superconducting phase transition close to the superconductor surface at the expense of the contact of the superconductor with a material characterized by the availability of high-Q lattice modes in the region of the superconducting gap (10–20 cm^{-1} for ordinary superconductors and 200-300 cm^{-1} for high-temperature superconductors) as well as at the expense of the comminution of the material and realization of a highly dispersed medium of the type of a globular photonic crystal.

These effects were studied in greater detail for ferroelectric crystals. As was demonstrated with KH_2PO_4 ferroelectric (KDP) [14], the interaction of acoustic vibrations with the optical soft mode strongly affected the acoustic and acousto-optical parameters of ferroelectric crystals with a linear relation of the order parameter (spontaneous polarization) and deformation through the piezoelectric effect. For the KDP the elastooptic constant P_{eff} increases sixfold in the vicinity of the phase-transition point at the expense of the energy transfer from the soft optical mode to the acoustic mode, while the acousto-optical efficiency $M_2 = P_{\text{eff}}/\rho\nu$ increases tenfold on the whole, since the phase transition is the ferroelastic one in this case. It should also be noted that the temperature difference $\Delta T = T_c - T_0$ characterizes the magnitude of this interaction and comprises $\Delta T = 4.7$ K for KDP [15].

The outlined relation of the fluctuations of the order parameter and deformation also results in the specific anisotropy of the acoustic anomalies in uniaxial ferroelectrics whose origin is the subject of considerable studies at present [16–20].

Note that the effect of the relation between the crystal vibrational modes and the fluctuations of the order parameter on the elastic and elasto-optical properties was studied mainly for ferroelectrics [14–

19]. Similar results should be expected for ferroelastics lacking a piezoelectric effect but with a linear interaction of the order parameter with a deformation allowed by symmetry.

2.2. Two-oscillator Model of the Phase Transition in Bismuth Vanadate

The phase transition in $BiVO_4$ was first reported in [21, 22] where this crystal was shown to be a ferroelastic. This means that at $T_c = 523$ K bismuth vanadate undergoes a phase transition of the second kind with change in the space symmetry group $I\,4_1/a \leftrightarrow I\,2/a$ or $4/mF2/m$ according to Aizu [23]. The $BiVO_4$ crystal belongs to "pure" ferroelastics since it is centrosymmetrical in both phases and lacks the anomaly in the temperature dependence of the permittivity $\varepsilon(T)$ [21] at the phase-transition temperature T_c.

The temperature studies of the separate Raman lines in bismuth vanadate [24] resulted in the detection of the temperature-dependent soft optical mode of symmetry B_g in the high-temperature phase. The squared frequency of this mode decreases linearly as the temperature decreases, $\omega^2 \propto (T - T_c)$, but does not vanish at the phase transition temperature. To analyze the Raman data, the authors of papers [24,25] speculated that the mean value of the normal coordinate Q served as the order parameter in this case, while the change in the crystal symmetry with the phase transition was associated with the irreducible representation B_g of the original group $C_{4h}\,(4/m)$. Thus, the crystal symmetry admits the linear in Q interaction between the order parameter and the elastic strain, whose components rearrange in the same manner as the order parameter. Because of this interaction, the optical mode induces the ferroelastic phase transition. The elastic modulus associated with the coordinate Q of the acoustic mode tends to zero at the temperature T_c, which appears to be greater than the phase-transition temperature of the system without regard for the interaction discussed (T_0). The spontaneous strain ε_B arising in this case distorts the unit cell of the high-temperature phase and reduces the crystal symmetry.

The strong coupling between the optical and acoustical vibrations in bismuth vanadate is confirmed by the results of neutron diffraction studies [26] and the manifestation of the soft acoustic mode in the spectra of Brillouin scattering [27–31]. However, these studies were carried out only for one scattering geometry. This prevented the study of the dynamics of the acoustical properties of $BiVO_4$ crystals in detail. Moreover, experimental data on the elastic moduli of the crystals under discussion and their temperature dependence have been lacking until the present paper.

In papers [32–35] the experimental and theoretical results of studies of the structural ferroelastic phase transition in bismuth vanadate were most fully systematized and a thermodynamic potential of the Landau type was constructed. The expansion of the difference of the Gibbs free energies of the two phases of bismuth vanadate into a power series of the order parameter Q has the form

$$\Delta G = \Delta G_{\text{opt}} + \Delta G_{\text{ac}} + \Delta G_{\text{int}} + \Delta G_{\text{ext}}. \tag{2.14}$$

Here,

$$\Delta G_{\text{opt}} = \frac{1}{2} m\omega_0^2 Q^2 + \frac{1}{4} BQ^4, \quad m\omega_0^2 = A_0(T - T_0), \tag{2.15}$$

$$\Delta G_{\text{ac}} = \frac{1}{2} C_{11}^0(\varepsilon_1^2 + \varepsilon_2^2) + \frac{1}{2} C_{33}^0 \varepsilon_3^2 + \frac{1}{2} + \frac{1}{2} C_{44}^0(\varepsilon_4^2 + \varepsilon_5^2)$$

$$+ \frac{1}{2} C_{66}^0 \varepsilon_6^2 + C_{12}^0 \varepsilon_1 \varepsilon_2 + C_{13}^0 \varepsilon_3(\varepsilon_1 + \varepsilon_2) + C_{12}^0 \varepsilon_6(\varepsilon_1 - \varepsilon_2) \tag{2.16}$$

is the contribution of the acoustic modes determined by the elastic energy $(1/2)C^0_{\mu\nu}\varepsilon_\mu\varepsilon_\nu$ [36],

$$\Delta G_{\text{int}} = -k_1 Q[m'(\varepsilon_1 - \varepsilon_2) + n'\varepsilon_6] - k_2 Q^2[m''(\varepsilon_1 + \varepsilon_2) + n''\varepsilon_3] - \frac{1}{2}k_3 Q(\varepsilon_4^2 - \varepsilon_5^2) - k_4 Q\varepsilon_4\varepsilon_5 \qquad (2.17)$$

is the interaction energy of the soft optical and acoustic modes, and

$$\Delta G_{\text{ext}} = -\sum_{\mu=1}^{6}\sigma_\mu\varepsilon_\mu = -\sum_{i,j=1}^{3}\sigma_{ij}\varepsilon_{ij} \qquad (2.18)$$

is the result of the effect of the external applied stresses.

Theoretical dependences of various spontaneous deformations on the temperature and pressure as well as similar dependences for the matrix of elastic moduli were calculated in [33] using the thermodynamic potential containing expressions (2.14)–(2.17) (without regard for external actions). The anomalous behavior of the acoustic properties of bismuth vanadate in the vicinity of the phase-transition point was predicted.

The study of the domain structure of $BiVO_4$ is of particular interest. The theoretical and experimental aspects of this structure were discussed in [37–43]. The transverse wave of acoustic deformation with propagation direction collinear to the domain walls of the crystal was shown [7] to be the acoustic soft mode with wave vector $\vec{q} = 0$. Because of this, the temperature studies of the domain-structure parameters provide information on the variation in the propagation direction of the soft acoustic modes in the crystal with temperature. Furthermore, this crystal provides a good example of the peculiar twinning in which the flat domain walls not only do not coincide with the symmetry-preferred directions but are not crystallograplic planes with rational Miller indexes at all. In this case, as indicated in [37], a temperature-dependent variation in the orientation of the domain walls should be observed, which are 90° only at $T = T_c$.

The theory of twinning in bismuth vanadate was constructed in [37] on the basis of [35, 38–42]. The temperature dependences of the domain-structure parameters were calculated in [35]. However, direct measurements of these parameters that would allow one to verify the conclusions of [35, 37] are lacking.

The number of domain types in $BiVO_4$ crystals is also a debatable point. In some papers (see, e.g., [41, 43]) only two types of domains were suggested. However, the existence of four types of domains in bismuth vanadate was predicted in [37, 42] and the compatibility conditions for the crystal structure at the boundaries of neighboring domains were obtained. From these conditions it follows that the domains should turn around with respect to each other since in each type of domain the crystal lattice basis is modified with respect to the basis of a paraelastic crystal phase in such a way as to prevent the lattice from rupturing when going to the ferroelastic phase. However, experimental studies of this type have not been performed earlier.

Thus, the effects of coupling of vibrational modes in bismuth vanadate and their effect on the elastic and elasto-optical properties of this crystal remain little known in spite of the number of papers [21–37, 41–46] devoted to the physical properties of $BiVO_4$ crystals.

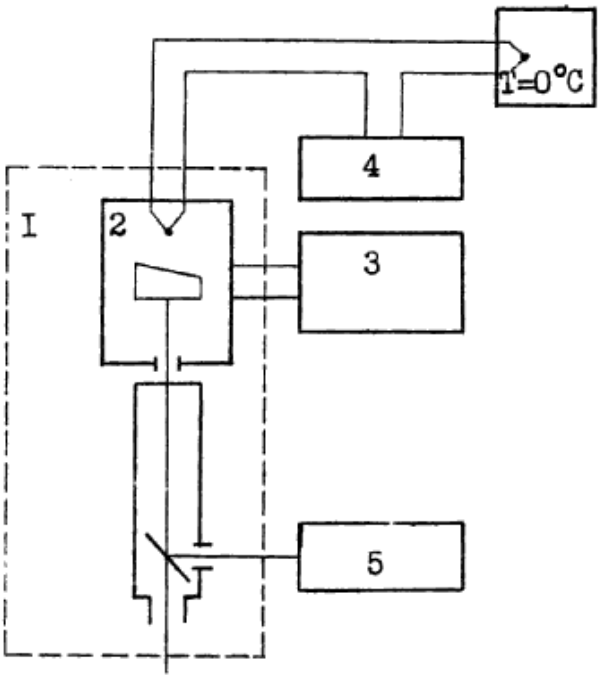

Fig. 3. Schematic diagram of the set-up for studies of the temperature dependences of refractive indices: 1) GS-5 goniometer, 2) optical thermostat, 3) heat controller, 4) temperature meter, and 5) laser.

3. Experimental Set-ups and Techniques Used

3.1. Set-up for Studies of Temperature Dependences of the Principal Refractive Indices

The autocollimating technique [47] was used to measure the refractive indexes. To study the temperature dependences of the refractive indexes of $BiVO_4$ crystals, a set-up was created based on the GS-5 goniometer. The schematic diagram of this set-up is shown in Fig. 3. A thermostat was positioned on the worktable of the goniometer. The thermostat table was rigidly mounted on the rotary table of the goniometer, while the thermostat case was rigidly connected with the stationary part of the goniometer. This gave immobility to the optical window of the thermostat with respect to the autocollimation tube of the goniometer. The temperature in the thermostat was set and maintained constant within 0.1 K during the time necessary for measurements with a thermostatic switch. A He–Ne laser LG-56 ($\lambda = 6328$ Å) was used as a light source. The control measurement for fused quartz provided the refractive index $n = 1.4572 \pm 0.0002$ at $T = 293$ K. This value agrees well with the data of [47] ($n = 1.45729 \pm 0.00004$).

3.2. Set-up for Measuring the Longitudinal Strain

Measurements of the longitudinal strain ε_3 were performed on the set-up shown in Fig. 4. It is based on the interference dilatometer as a modified Michelson interferometer with the use of the prism as a dividing mirror. An LG-78 He-Ne laser ($\lambda = 6328$ Å) was used as a light source.

A laser beam 4 was incident on one of the lateral faces of a prism 3 and was divided at its semi-

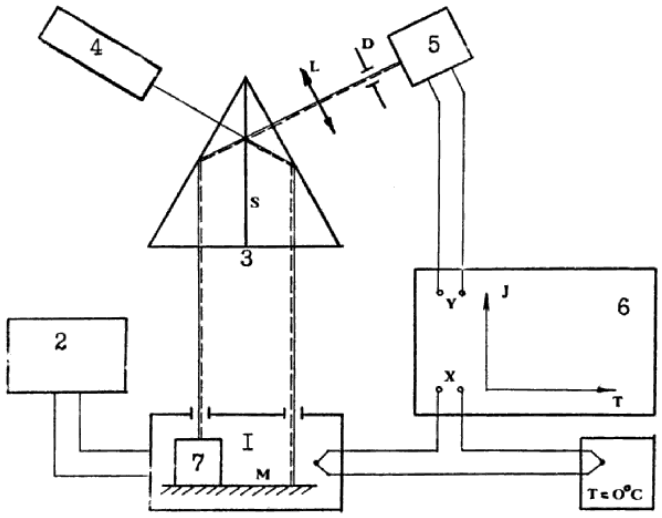

Fig. 4. Schematic diagram of the set-up for measuring longitudinal strains: 1) optical thermostat, 2) thermostatic switch, 3) prism, 4) laser, 5) photodetector, 6) XY-recorder, and 7) sample.

transparent boundary S into two beams 1 and 2 equal in intensity. The beam 1 was reflected from the boundary S and from the entrance lateral face of the prism, emerged through the prism base normal to its surface, and was incident normally upon one of the parallel faces of the sample under study. Reflecting from the sample surface, it traveled the same path to the boundary S where it was divided in two again. A portion of radiation was returned to the laser, while the other portion (beam $1'$) passing through the boundary S was perpendicular to the other lateral prism face. The beam 2 passing through the transparent boundary S was reflected from the second lateral prism face, emerged from it normally to the prism base, and impinged normally on the mirror surface made coincident with the other plane-parallel face of the sample studied. Reflecting from the mirror, the beam 2 traveled the same path to the boundary S where it was divided into two. A portion of radiation passing through the boundary S was returned to the laser, while the other portion (beam $2'$) impinged normally on the other lateral prism face. The beams $1'$ and $2'$ traveling nearly the same optical path were collected by a lens and produced a stable interference pattern. The smooth variation in one of the optical paths (elongation of the sample because of thermal expansion and contraction) resulted in motion of the interference pattern. Such an optical arrangement allowed one to measure the variation in the path-length difference of the beams reflected from the parallel faces of the plane-parallel plate and provided high stability of the interference pattern due to the small spatial separation of the interferometer arms.

The $BiVO_4$ sample and mirror were placed in the optical thermostat to measure the temperature dependence of the longitudinal strains. The temperature in the thermostat was set and maintained constant within 0.1 K. A differential chromel–alumel thermocouple was used as a temperature probe. The voltage from the thermocouple was applied to the X-input of the recorder. The variation in the light intensity determined by the motion of the interference pattern was detected by the photodetector. The signal from the photodetector was fed into the Y-input of the recorder. The temperature dependence of the elongation of the crystal was recorded on the plane-table of the XY-recorder. The strain ε_3 was calculated by the formula $\varepsilon_3 = \Delta l/l = m\lambda/2l$, where Δl is the change in the length l of the crystal

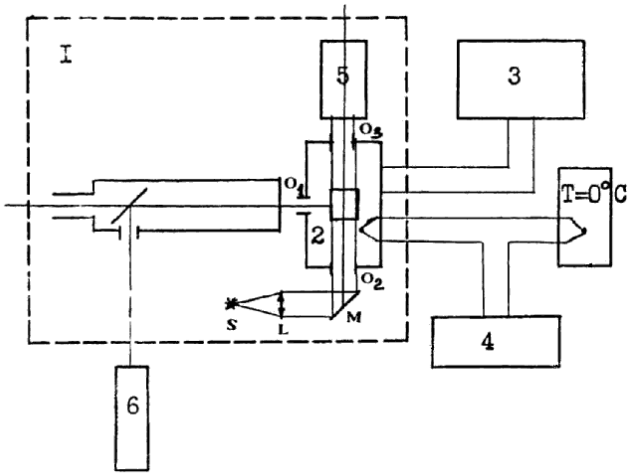

Fig. 5. Schematic diagram of the set-up for measuring shear strains and studies of the domain structure parameters of $BiVO_4$ crystals: 1) GS-5 goniometer, 2) optical thermostat, 3) thermosatic switch, 4) temperature meter, 5) MBS-1 microscope, 6) laser, and S, L, and M are the components of the illuminating system (S is the lamp, L is the lens, and M is the turning mirror).

along the Z axis ($l = 4$ mm), m is the number of orders of interference crossing the entrance slit of the photodetector D, and $\lambda = 6328$ Å is the wavelength of the light source.

3.3. Set-up for Studies of Temperature Dependences of the Domain-Structure Parameters and Measurements of the Components of the Spontaneous-Strain Tensor

The temperature dependences of the slope of the domain boundary W' with respect to the crystallographic direction [010] $p(T)$ and of the difference of the angle between the domain walls from 90° $\mu(T)$ as well as the components of the spontaneous-strain tensor of the crystal were measured on the same set-up that was used for the measurements of the principal refractive indexes. For this purpose the set-up was supplemented with a MBS-1 microscope mounted on the stationary part of the GS-5 goniometer. A thermostat with three optical windows O_1, O_2, and O_3 (see Fig. 5) was mounted on the worktable of the goniometer.

The thermostat table with the crystal under study mounted on it was rigidly bound with the goniometer worktable, while the thermostat case and MBS-1 microscope were rigidly bound with the stationary part of the goniometer. This made the window O_1 immobile with respect to the autocollimator, whereas the sample under study could be rotated by any angle. Such a method allowed one to measure the variation in the angles between the portions of the lateral prism faces associated with different domains with an accuracy of $10''$–$20''$. At the same time, the domain boundaries of the sample under study could be observed through the windows O_2 and O_3 using the microscope and illuminating system S, L, and M (see Fig. 5).

The dependences $p(T)$ and $\mu(T)$ were measured in the following manner. The particular temperature was set and maintained constant within 0.1 K by the thermostatic switch during the time necessary for the measurement. Then the cross-hairs of the microscope eyepiece were consecutively made coincident

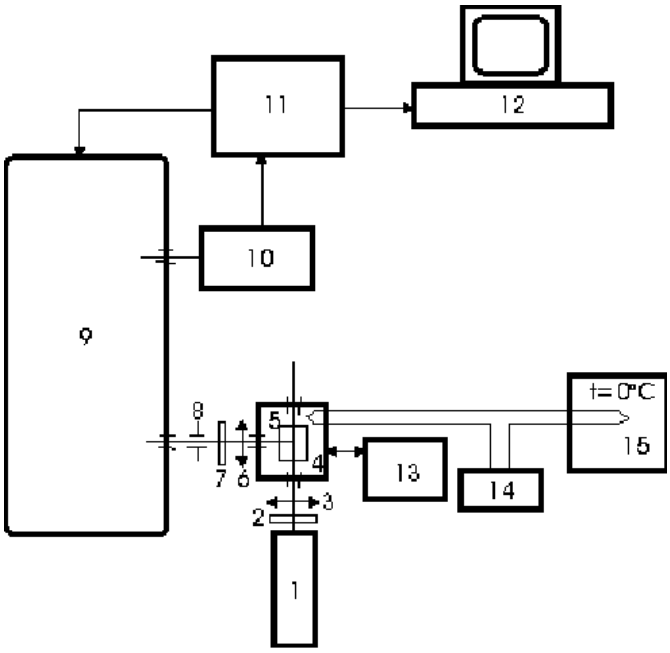

Fig. 6. Schematic diagram of the automated Raman spectrometer: 1) LG-38 laser, 2) polarizer, 3) and 6) objectives, 4) optical thermostat, 5) sample, 7) analyzer, 8) diaphragm, 9) DFS-12 spectrometer, 10) photomultiplier tube and pulse shaper, 11) interface block, 12) computer, 13) thermostatic switch, 14) temperature meter, and 15) thermos flask with thawing ice.

with the directions measured by turning the goniometer table. The difference in the goniometer readings yielded the desired angle. The measurement error was defined by the accuracy of coincidence of the eyepiece cross-hairs with the image of the domain boundary or the edge of the prism and was $\pm 5'$. The temperature dependence of the components of the spontaneous-strain tensor of the single-domain crystal of bismuth vanadate was determined from the measured temperature dependence of the change in the prism angle. The latter was used previously for studies of the temperature dependences of the principal refractive indexes. The prism angles were measured by the autocollimating technique through the optical window O_1. In this case, the accuracy of measuring the angles was $10''$–$20''$.

3.4. Set-up for Studies of Temperature Dependences of Raman Spectra in Bismuth Vanadate Crystals

The optical soft mode was studied on the automated Raman spectrometer. Its schematic diagram is shown in Fig. 6. The sample under study 5 was placed into an optical thermostat 4. The temperature in the thermostat was set and maintained within 0.1 K during the time necessary for the spectrum to be recorded using the thermostatic switch 13. The temperature was measured with a chromel–alumel differential thermocouple whose cold junction was kept at a temperature $T = 0°$C. The Raman spectra were excited in the sample with the radiation of a He–Ne laser 1 ($\lambda = 6328$ Å, exciting power 20 mW). The image of the scattering volume was formed by an objective 3 at the entrance slit of an automated Raman spectrometer 9 controlled with a computer 12 through the interface block 11. Polarizers 1 and 6 were used to realize the necessary polarization geometry of Raman scattering. A diaphragm 8

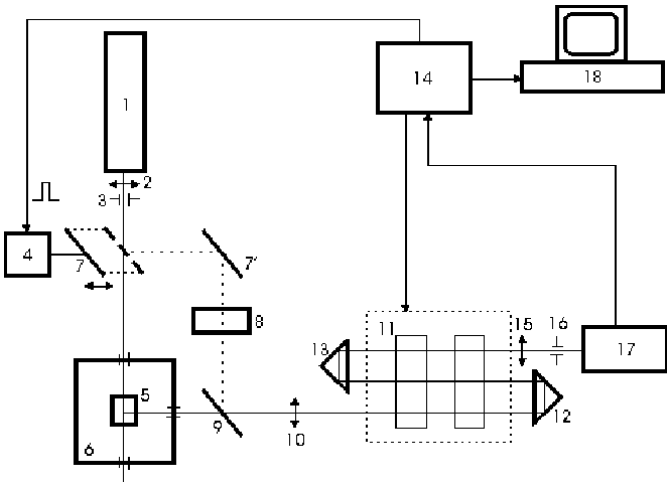

Fig. 7. Schematic diagram of the automated spectrometer for Brillouin scattering: 1) laser, 2) focusing lens, 3) diaphragm, 4) magnetic switch, 5) sample, 6) optical thermostat, 7) movable mirror, 7′) turning mirror, 8) diffuser filter, 9) glass plate, 10) and 15) collecting optics, 11) Fabry-Perot interferometer, 12) and 13) corner reflectors, 14) interface block for the control unit of the Fabry-Perot interferometer, 16) output diaphragm, 17) photomultiplier tube and pulse shaper, and 18) computer.

eliminated glares associated with the diffuse scattering at the sample boundaries. The Raman spectra were detected with an FEU-79 photomultiplier tube operating in the single-electron mode. The pulses from the photomultiplier tube were converted by a pulse shaper 10 and were fed into the counter in the interface block. The counting time was set by software. The spectrum detected was displayed on the screen, with subsequent recording into the memory of a computer 12.

3.5. Set-up for Studies of Temperature Dependences of Parameters of the Acoustical Modes in Bismuth Vanadate

A schematic diagram of the set-up used in studies of acoustical soft modes is shown in Fig. 7. The set-up consisted of a scanning Fabry-Perot interferometer 11 controlled by a computer 18 through an interface block 14, an optical thermostat 6 with a system of stabilization and temperature measurement (not shown in Fig. 7), an optical modulator 4-7-7′-8-9, an LG-38 laser 1 (λ = 6328 Å, exciting power 20 mW), and a photon counter 17. A sample 5 was mounted in the optical thermostat equipped with a system of stabilization and temperature measurement. The design, operation, and characteristics of this system are described above (see Fig. 6). Radiation of the laser 1 was focused by a lens 2 in such a way that the beam focal waist was within the sample under study and at the focus of a lens 10. The scattered light passed through a Fabry–Perot interferometer 11 three times, reflecting from corner reflectors 12 and 13. The image of the isoclinic rings was focused by an objective 15 and through a diaphragm 16, and an interference filter fell on the photocathode of the FEU-136 photomultiplier tube operating in the photon counting mode. The pulses from the photomultiplier tube converted by a pulse shaper 17 arrived at the counter in the interface block 14. The counting time was set by software. The spectrum recorded appeared on the display of the computer 18. The scanning and automatic tuning of the Fabry-Perot interferometer was performed by a digital-to-analog converter in the interface block through a specially designed three-channel high-voltage amplifier (control unit of the Fabry-Perot interferometer).

The optical modulator was included in the set-up for adjustment and automatic tuning of the Fabry-Perot interferometer without changing the sample position. It was controlled by software and consisted of a light chopper 4 with a moving mirror 7, a turning mirror 7′, a diffuser filter 8, and a plane-parallel glass plate 9. With this modulator, light passed through the interferometer, by-passing the sample when manual adjustment and self-tuning of the Fabry-Perot interferometer were necessary, as well as when passing the central peaks and in reverse motion. This allowed one to choose the intensity of the central peaks optimum for the adjustment program using a filter 8.

4. Relation of the Physical Properties of $BiVO_4$ Crystals with Variations in the Order Parameter

4.1. Studies of the Spontaneous Strain of a Single-domain $BiVO_4$ Crystal

Data on the temperature dependences of the refractive indexes and order parameter, i.e., of the spontaneous strain, are necessary for the quantitative description of characteristics of light scattering in crystals. The techniques for measuring these quantities for $BiVO_4$ crystals were described earlier in [29, 48–53].

In the case of the ferroelastic phase transition the spontaneous strain is the order parameter. As mentioned above, the phase transition in bismuth vanadate is induced by the soft optical mode whose normal coordinate according to [35] is associated with a displacement of Bi^{3+} ions and is transformed by the B_g representation of the initial symmetry group C_{4h}. Interaction of this mode with the acoustic mode ε_B of the same symmetry results in "condensation" of this mode [25]. This gives rise to the spontaneous strain ε at $T < T_c$. This strain distorts the unit cell of the high-temperature (paraelastic) phase and transforms it from the tetragonal cell (with the parameters a_T and c_T) to the monoclinic one (with the parameters a_M, b_M, c_M, and γ) [35],

$$\varepsilon_s = \begin{pmatrix} -a & b & 0 \\ b & a & 0 \\ 0 & 0 & 0 \end{pmatrix}, \quad \text{where} \quad a = \frac{a_M - b_M}{a_T}, \quad b = \tan\left(\frac{90^\circ - \gamma}{2}\right). \tag{4.1}$$

In this case, the spontaneous strain of the low-temperature (ferroelastic) phase has the form $\varepsilon_B = m(\varepsilon_1 - \varepsilon_2) + n\varepsilon_6$, while the acoustic soft mode in the paraelastic phase contains the combinations $(\varepsilon - \varepsilon_2)$ and ε_6. These combinations are transformed by the B_g representation of the symmetry group C_{4h} [31,33] and correspond to the shear strain of the crystal [36].

The proposed mechanism of the phase transition in $BiVO_4$ also assumes the strong coupling of the soft optical mode with the acoustic one ε_A. The strain components of the latter are transformed by the unit representation A_g of the initial symmetry group C_{4h} and have the form $\varepsilon_A = \varepsilon_1 + \varepsilon_2 + \varepsilon_3$.

The temperature dependences of spontaneous strains were studied in single-domain and polydomain crystals of bismuth vanadate. Both the shear strains of the symmetry B_g, $\varepsilon_B = m(\varepsilon_1 - \varepsilon_2) + n\varepsilon_6$, and the longitudinal strains of the symmetry A_g, ε_A, were measured in single-domain $BiVO_4$ samples. The shear strains were measured from the change in the angle of the prism cut from the single-domain $BiVO_4$ crystal. The temperature measurements of some components of the spontaneous strain tensor were carried out for a polydomain crystal of bismuth vanadate.

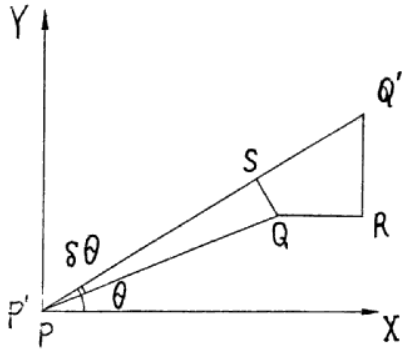

Fig. 8. Variation in the angle θ on the strain in the crystal.

Let us consider the linear element $\delta\vec{r} = PQ$ (see Fig. 8) to determine $\delta\theta$, the variation in the angle θ between the direction $[\cos\theta, \sin\theta, 0]$ in the crystal and the X axis under the action of spontaneous strain. If the displacement of the point P is defined by the vector $\vec{u}$, then the displacement of the point Q is

$$\vec{u} + \frac{\partial\vec{u}}{\partial r} = \vec{u} + \hat{\omega}\cdot\delta\vec{r} + \hat{\varepsilon}\cdot\delta\vec{r},$$

where

$$\varepsilon_{ij} = \frac{1}{2}\left(\frac{\partial u_i}{\partial x_j} + \frac{\partial u_j}{\partial u_i}\right)$$

is the tensor of small strains, and

$$\omega_{ik} = \frac{1}{2}\left(\frac{\partial u_i}{\partial x_k} + \frac{\partial u_k}{\partial u_i}\right)$$

is the tensor of small rotations.

Since $QR = \sum\limits_k(\omega_{1k} + \varepsilon_{1k})\delta x_k$, $RQ' = \sum\limits_k(\omega_{2k} + \varepsilon_{2k})\delta x_k$, and $QS = -QR\sin\theta + RQ'\cos\theta$, we obtain

$$\delta\theta = \frac{QS}{\delta R} = \omega_{21} + \frac{1}{2}(\varepsilon_{22} - \varepsilon_{11})\sin 2\theta + \varepsilon_{12}\cos 2\theta. \tag{4.2}$$

Expression (4.2) is valid both for single-domain and polydomain crystals.

A single-domain $BiVO_4$ sample was used for measurement of the shear spontaneous strain of the symmetry B_g, $\varepsilon_B = m(\varepsilon_1 - \varepsilon_2) + n\varepsilon_6$. It represented a right-angle prism with the lateral faces normal to the symmetry plane (001) of the crystal and forming the angles $\theta_1 = 105^\circ$ and $\theta_2 = 114^\circ$ with the positive direction of the X axis. The temperature dependence of the prism angle formed by these faces was measured on the set-up for measurements of the refractive indexes described in [53]. One can show using Eq. (4.2) that the variation in the prism angle caused by the strain ε_B is equal to

$$\Delta\varphi = a(\sin 2\theta_2 - \sin 2\theta_1) + b(\cos 2\theta_2 - \cos 2\theta_1), \tag{4.3}$$

where

$$a = \frac{a_M - b_M}{2a_T} \quad \text{and} \quad b = \tan\left(\frac{90^\circ - \gamma}{2}\right).$$

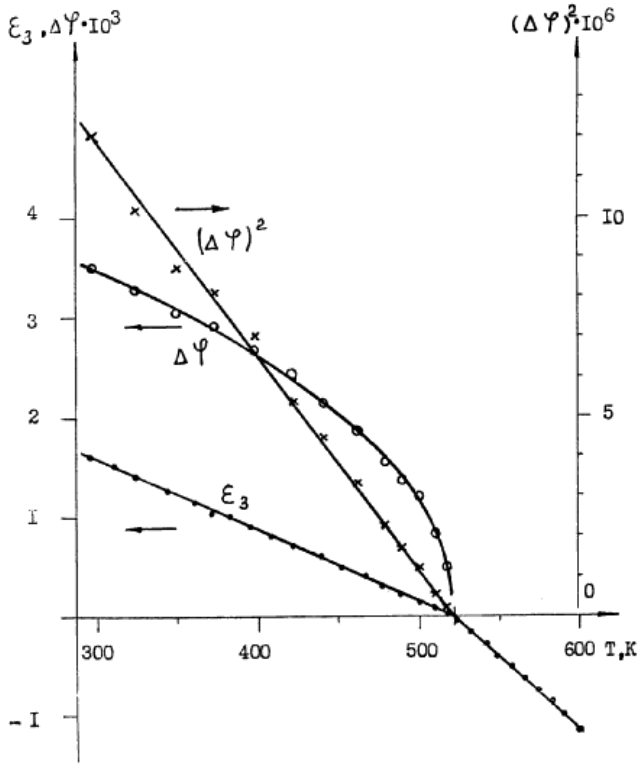

Fig. 9. Temperature dependence of the strain ε_3 and of the parameters $\Delta\varphi$ and $(\Delta\varphi)^2$.

With parameters of the tetragonal cell a_T and of the monoclinic cell a_M, b_M, and γ at $T = 300$ K taken from [35], we obtain $\Delta\varphi = 3.1 \cdot 10^{-3}$. This value agrees satisfactorily with $\Delta\varphi = 3.5 \cdot 10^{-3}$ obtained by us [48]. Figure 9 presents the experimental temperature dependences $\Delta\varphi \sim \varepsilon_B$. One can see that the temperature dependence of the strain ε_B can be approximated by the function $(T_c - T)^{1/2}$ in the temperature range 300–522 K.

The temperature dependence of the longitudinal strain ε_3 belonging to the symmetry type A_g was measured on the set-up whose mode of functioning was described in [48]. The experimental temperature dependence of the strain ε_3 is shown in Fig. 9. As the temperature varies from 295 to 566 K, the elongation of the crystal is $1.8{\cdot}10^{-3}$ [48]. This result agrees satisfactorily with the value $1.8{\cdot}10^{-3}$ calculated from the data of [49]. The coefficient of linear expansion of the crystal changes stepwise at $T = T_c$ from the value $\alpha_1 = (18.9 \pm 0.6) \cdot 10^{-6}$ deg^{-1} to $\alpha_2 = (5.3 \pm 0.1) \cdot 10^{-6}$ deg^{-1} because of the spontaneous strain ε_3 arising at $T < T_c$.

For the analysis of the results obtained we use the expansion in terms of Q, ε_B, and ε_3 of the portion of the free energy density of the crystal, which depends on these variables,

$$F - F_0 = \frac{1}{2}A_0(T - T_0)Q^2 + \frac{1}{4}BQ^4 + k_B\varepsilon_B Q + k_3\varepsilon_3 Q^2 + \frac{1}{2}C_B\varepsilon_B^2 + \frac{1}{2}C_{33}^0\varepsilon_3^2. \qquad (4.4)$$

Here, the constants A_0, B, k_B, k_3, C_B, and C_{33}^0 are perceived to be independent of temperature. The first and last two terms of expansion (4.4) correspond to the energy of optical and acoustic phonons of the

B_g and A_g symmetries, while the third and fourth terms characterize the relation of the corresponding modes. Using the equilibrium conditions

$$\frac{\partial F}{\partial Q} = 0, \quad \frac{\partial F}{\partial \varepsilon} = 0,$$

we obtain the equilibrium values of the strain and the order parameter,

$$Q_0^2 = \begin{cases} 0 \quad \text{with} \quad T \geq T_c, \\ -\dfrac{A(T - T_c)}{B(1 - x)} \quad \text{with} \quad T < T_c, \end{cases} \quad \varepsilon_B = -\frac{k_B}{C_B} Q_0, \quad \varepsilon_3 = -\frac{k_3}{C_{33}^0} Q_0^2. \tag{4.5}$$

Here, $x = 2k_3^2/BC_{33}^0$ and $T_c - T = k_A^2/AC_B$ are the parameters that characterize the relation of the acoustic modes ε_B and ε_3 to the optical soft mode. The experimental temperature dependences of the spontaneous strains ε_B and ε_3 (see Fig. 9) support linear and quadratic dependences of the equlibrium values of strains of B_g and A_g symmetry types and of the order parameter predicted by the theory. The linear dependences $(\Delta\varphi)^2$ and ε_3 (see Fig. 9) correspond to the presumed temperature dependence of the strains ε_A and ε_B and demonstrate that the behavior of the order parameter in $BiVO_4$ within the temperature range 300–600 K correlates with the Landau theory. Our experimental data [48] are indicative of the strong relation between the elastic strains ε_A and ε_B and the order parameter. This supports the mechanism of the phase transition in $BiVO_4$ proposed in [25].

4.2. Temperature Dependence of the Domain-Structure Parameters and Spontaneous Strain of Polydomain $BiVO_4$ Crystals

The acoustic soft modes were shown [35] to propagate in $BiVO_4$ crystals along directions collinear to the directions of the domain boundaries. It will suffice to study the temperature behavior of the domain boundaries to obtain information on the variation in the propagation direction of acoustic modes in the crystal with temperature.

Furthermore, as mentioned above, the domain structure of bismuth vanadate shows that the unusual twinning type is defined by the spontaneous strain of the crystal rather than occurs along symmetry-preferred crystallographic directions. As was shown in [37, 39], the orientation of the domain boundaries and the angle between them should be temperature dependent. It was shown [37] on the basis of the macroscopic strain compatibility conditions at the domain boundaries [39] that formation of the two types (S_1 and S_2) of domains in $BiVO_4$ was possible at $T = T_c$. In this case, 90° plain boundaries are formed whose orientation $(p, 1, 0)$ and $(1, -p, 0)$ with respect to the crystal coordinate system of the prototype is determined by the components of spontaneous strain,

$$p = [b + (a^2 + b^2)^{1/2}]a^{-1}, \tag{4.6}$$

where

$$a = \frac{a_M - b_M}{2a_T}, \quad b = \tan\left(\frac{90^\circ - \gamma}{2}\right). \tag{4.7}$$

Relationship (4.6) was obtained under the assumption that the components of spontaneous strain of all possible orientation states S_1 and S_2 at $T = T_c$ were associated with rotation through the angle $\pi/2$ (C_4 is the symmetry element, which is lost during the phase transition). It is not the case at $T < T_c$, and

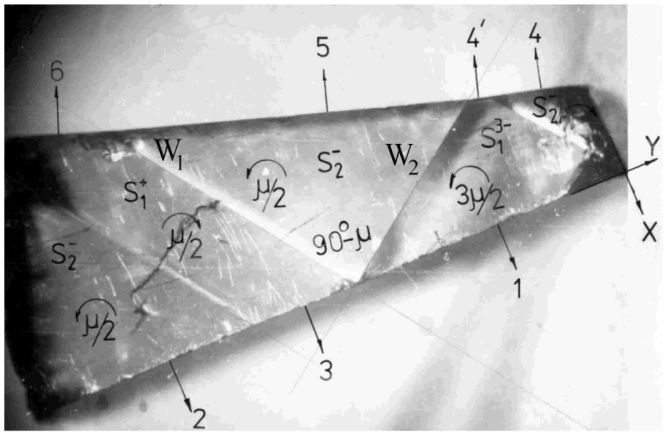

Fig. 10. View of the polydomain $BiVO_4$ crystal in the plane (001) at $T = 300$ K. Figures 1–6 denote the normals to the exterior faces of the domains.

the macroscopic condition of coherence of the domain boundary [37] should be used to find the orientation of the domain walls. In this case, relationship (4.6) remains valid when considered with respect to the nonorthogonal coordinate system of monoclinic syngony. Additional rotation of the adjacent domains through the angle $\pm\mu/2$ is required for their compatibility. This angle is defined by the spontaneous strain [37, 40, 42],

$$\tan\mu = 2(a^2 + b^2)^{1/2}. \tag{4.8}$$

Thus, because of the temperature dependence of spontaneous strain, the orientation of the domain boundaries (defined by the value of p) and the angle between them (which is equal to $\pi/2 \pm \mu$) should also be temperature dependent.

With consideration for the relative rotation of the adjacent domains through the angle $\mu/2$, the tensor of spontaneous strain can be written as follows [37, 40, 42]:

$$\varepsilon^s(S) = \pm \begin{pmatrix} -a & b \\ b & a \end{pmatrix} \pm \begin{pmatrix} 0 & \mu/2 \\ -\mu/2 & 0 \end{pmatrix}. \tag{4.9}$$

In what follows we omit the insignificant components of ε^s, since the domain boundaries are parallel to the symmetry axes of the crystal and the problem can be considered as a two-dimensional one. Various combinations of signs in (4.9) correspond to the four possible orientation states, which are designated as S_1^+, S_2^+, S_1^-, and S_2^-. In this case, the states with different superscripts indicating the directions of domain rotation should be compatible.

We use the $BiVO_4$ sample in the form of a right-angle prism with the base parallel to the (001) symmetry plane of the crystal to measure the temperature dependences $p(T)$ and $\mu(T)$ and compare them with the theoretical ones [37]. The sample was divided into several large domains. Both types of domain boundaries were observed in this case (see Fig. 10). The angle between the domain boundaries and the angle θ between the direction of the domain boundary W_1 and the prism edge [direction (010)] were measured on the set-up described earlier [50].

Our measurements provide the values $\mu = 1.2°$, $\theta = 35.0°$, and $p = 0.70 \pm 0.02$ at $T = 300$ K [50]. These values correlate well with both the calculated ones ($\mu = 1.2°$, $\theta = 35.7°$, and $p = 0.72$) and those

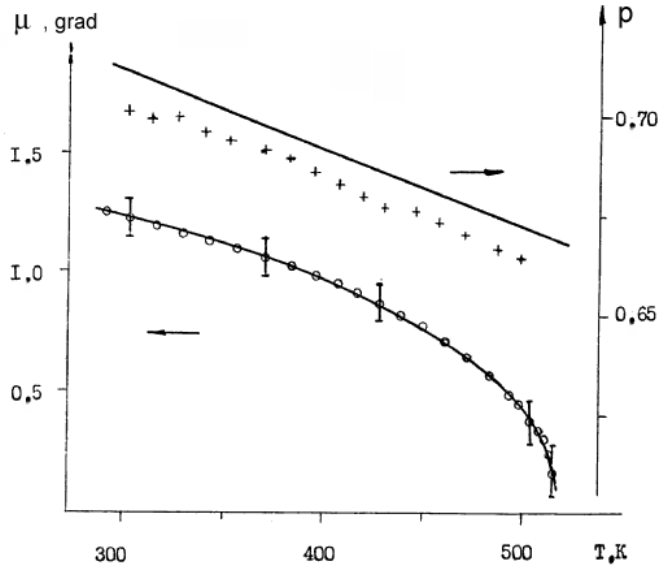

Fig. 11. Temperature dependences of the domain-structure parameters of $BiVO_4$, $p(T)$ and $\mu(T)$. The solid lines correspond to the dependences calculated by relationships (4.6) and (4.7).

found in [42] ($\mu = 1°$, $\theta = 37.4°$, and $p = 0.78$) and [41] ($p = 0.735$). The main error in the determination of the parameter p is associated with poor accuracy ($\sim 1°$) of the sample orientation with respect to the crystal coordinate system. The components of the spontaneous strain tensor obtained in x-ray diffraction studies [35] were used in the calculations of the parameters p and μ and their temperature dependences. The temperature in the thermostat was varied and fixed with an accuracy of 0.1 K to construct the temperature dependences $p(T)$ and $\mu(T)$. The character of the domain structure in the crystal does not change with increase in the temperature up to 160°. The formation of smaller domains starts at $T > 160$°C. Their number rapidly increases with temperature while the dimensions decrease. The domain walls W_1 and W_2 observed at room temperature can be discerned up to the temperature of 243°. At this temperature the whole sample is divided into small domains that prevent further measurements. The reverse situation is observed with cooling and at room temperature the crystal reverts to the original state. This is indicative of a pinning of domains on lattice imperfections.

Figure 11 shows the temperature dependences $p(T)$ and $\mu(T)$ obtained as a result of averaging three sets of measurements. The coincidence of the experimental points [50] with the calculated curves (solid lines in Fig. 11) is indicative of good agreement between theory and experiment. The small shift of the dependence $p(T)$ is presumably due to the systematic error resulting from inaccuracy in sample alignment.

4.3. Spontaneous Strain in $BiVO_4$ Polydomain Crystals

As is discussed below, the technique of studying the spontaneous strain of polydomain bismuth vanadate crystals proposed in [52, 53] provides a possibility of measuring both the symmetrical and antisymmetrical parts of the distortion tensor components.

The bismuth vanadate crystal under study represented a right-angle prism with dimensions of several

millimeters and base parallel to the (001) symmetry plane of the crystal. The prism was cut from the single-domain $BiVO_4$ crystal, polished, and used in the preliminary experiments on measurement of the temperature dependence of the refractive indexes of the crystal [53]. During the measurement the crystal was transformed into the polydomain phase as a result of cooling down to $T = T_c$. Six large domains were formed at $T = 300$ K. They included all possible types of domains.

Figure 10 shows a view of the sample in the (001) plane and the relative position of the domains. As is seen from this figure, two types of nearly perpendicular domain walls occur in the sample. The first type corresponds to the boundary of the orientation states S_2^- and S_1^+. The second type of domain boundary, which includes the orientation states S_2^- and S_1^{3-}, corresponds to the domain wall nearly perpendicular to that of the first system. In this case, the compatibility of the S_1^{3-} domain requires its rotation through the angle $-3\mu/2$. This state designated as S_1^{3-} is compatible with the state S_2^- and is not compatible with the state S_1^+, since they are turned with respect to each other through the angle 2μ.

Substituting the distortion tensor for various orientation states (4.9) into (4.2) we find the angles between the portions of the lateral face of the prism that belong to the corresponding domains. Using for these angles the same notation as in Fig. 10, we obtain for the S_1^+ and S_2^- domains

$$\Psi_{32} = \delta\theta_1(S_1^+) - \delta\theta_1(S_2^-) = -\mu + 2a\sin 2\theta_1 + 2b\cos 2\theta_1, \tag{4.10}$$

$$\Psi_{56} = \delta\theta_2(S_1^+) - \delta\theta_2(S_2^-) = -\mu + 2a\sin 2\theta_2 + 2b\cos 2\theta_2. \tag{4.11}$$

For the domains S_1^+ and S_1^{3-} we similarly find

$$\Psi_{31} = \delta\theta_1(S_1^+) + \delta\theta_1(S_1^{3-}) = 2\mu. \tag{4.12}$$

The lateral faces of the crystal studied were defined by the angles $\theta_1 = 90^\circ$ and $\theta_2 = -108^\circ$. This enabled us to calculate the parameters a, b, and μ measuring the angles Ψ_{31}, Ψ_{32}, and $\Psi_{44'} = \Psi_{56}$. The values of the angles $\Psi_{31} = 2^\circ 28'$, $\Psi_{32} = 1^\circ 38'$, $\Psi_{44'} = 51'$, and $\Psi_{56} = 52'$ measured at $T = 300$ K agree well with those $\Psi'_{31} = 2^\circ 25'$, $\Psi'_{32} = 1^\circ 35'$, and $\Psi'_{44} = \Psi'_{56} = 50'$ calculated by formulas (4.10)–(4.12). The lattice parameters of $BiVO_4$ obtained from the x-ray diffraction studies [35] were used to calculate the components of the strain tensor a, b, and μ.

Measurement of the temperature dependences of the angles Ψ_{31}, Ψ_{32}, and Ψ_{56} enabled us to calculate the temperature dependences of the angle μ characterizing the deviation of the angle between the domain walls from 90° (the asymmetric part of the strain tensor) as well as of the components of spontaneous strain $a(T)$ and $b(T)$. The temperature dependences of these parameters obtained and the calculated values of $a^2(T)$, $b^2(T)$, and $(\mu/2)^2(T)$ are presented in Figs. 12 and 13. The angles obtained from averaging three sets of temperature measurements were used in the calculations. In this case, the mean deviations were 0.2%, 2%, and 10% at the temperatures of 300 K, 470 K, and 510 K, respectively. The results of our measurements of $(\mu/2)^2(T)$, $a^2(T)$, and $b^2(T)$ [51,52] agree well with the results of the x-ray diffraction measurements (shown in Fig. 13 by the solid lines) obtained on single-domain samples [35]. It should be noted that x-ray diffraction studies prevent the antisymmetric part of the spontaneous strain tensor from being determined.

4.4. Temperature Dependences of the Principal Refractive Indices of $BiVO_4$

A single-domain crystal of bismuth vanadate was used for studies of the temperature dependences of the principal refractive indexes. This crystal represented a tetrahedral right-angle prism with dimensions

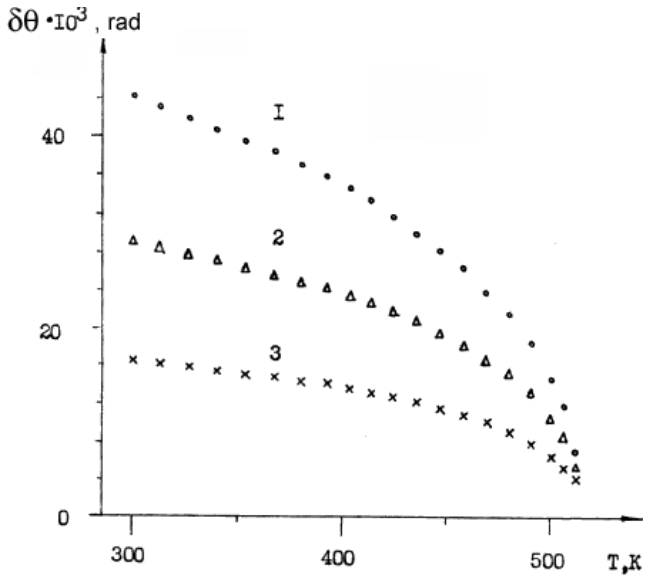

Fig. 12. Temperature dependences of the angles Ψ_{31} (1), Ψ_{32} (2), and Ψ_{56} (3) for a polydomain $BiVO_4$ crystal.

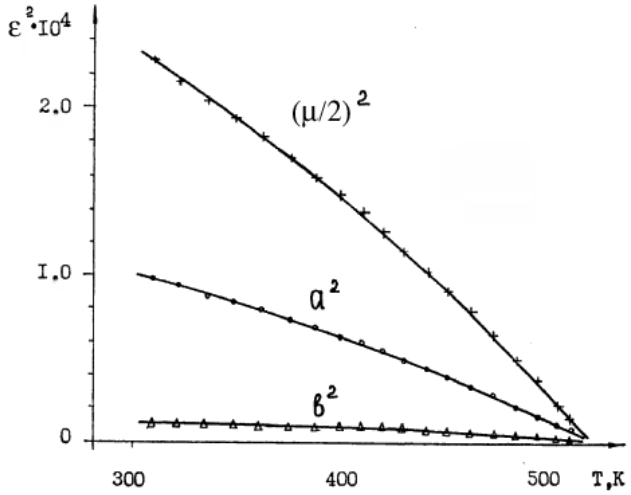

Fig. 13. Temperature dependences of the parameters a^2, b^2, and $(\mu/2)^2$. The solid lines show the results obtained from the x-ray diffraction measurements of single-domain samples [35].

of $4 \times 4 \times 6$ mm and the base parallel to the crystal symmetry plane (001). The directions of the axes of the optical indicatrix were determined from the polarization measurements. According to these measurements, the axes N_1 and N_2 are turned in the crystal symmetry plane (001) through an angle of $24^\circ \pm 1^\circ$ with respect to the crystallographic axes a and b. For this reason the prism was cut out in such a way that the two adjacent faces (with the angle between them 90°) were coincident with the directions of the N_1 and N_2 axes, while the prism angles between the opposite faces were smaller than 18°. This was done to prevent the total internal reflection of the rays, since the Brewster angle was about 72° with

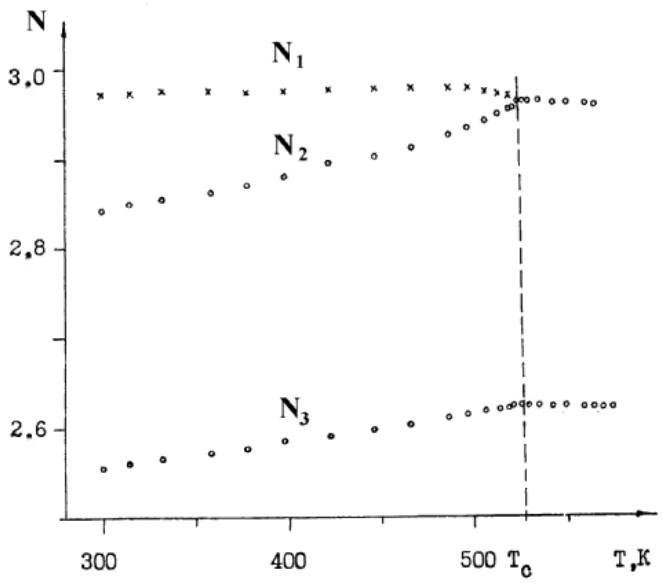

Fig. 14. Temperature dependences of the principal refractive indices of $BiVO_4$.

a refractive index of 2.8.

The principal refractive indexes of bismuth vanadate measured at $T = 293$ K were $N_1 = 2.971 \pm 0.002$, $N_2 = 2.842 \pm 0.002$, and $N_3 = 2.555 \pm 0.002$. From this it follows that the crystal is optically negative and the angle between its optical axes is $2V = 118°$.

The results of temperature measurements of the principal refractive indexes of $BiVO_4$ are presented in Fig. 14. These measurements ignore a small ($< 2°$) variation in the turning angle of the axes of the optical indicatrix in the plane (001) [32]. With $T < T_c$ the refractive indexes N_1 and N_2 vary linearly with temperature up to the value $N_0 = 2.962$, while N_3 increases linearly up to the value $N_e = 2.623$. With $T > T_c$ the refractive indexes depend only slightly on the temperature. Their temperature coefficients are $\alpha_0 = -1.5 \cdot 10^{-4}$ deg^{-1} and $\alpha_e = -6 \cdot 10^{-5}$ deg^{-1}. The drastic increase in the absorption of light polarized in the plane (001) with the sample temperature is observed. The intensity of light passing through the crystal drastically decreases at $T > 600$ K.

The temperature dependence of the refractive indexes N_i can be associated with the variation in the permittivity tensor δB_a under the action of the temperature-dependent spontaneous strain because of the elasto-optical effect, $\delta B_a = P_{\alpha\beta}\varepsilon_\beta$. The diagonal reduction of the tensor δB_a allows one to find its principal values δb_i and to determine the variation in the principal refractive indexes $\delta N_i = -N_i^2 \delta b_i/2$:

$$\delta N_{1,2} = -\frac{N_0^3}{4}\left\{[(p_{11}+p_{22})(\varepsilon_1+\varepsilon_2)+p_{13}\varepsilon_3\right.$$

$$\left.\pm\{[(p_{11}-p_{22})(\varepsilon_1-\varepsilon_2)+2p_{12}\varepsilon_6]^2+4[p_{61}(\varepsilon_1-\varepsilon_2)+p_{66}\varepsilon_6]^2\}^{1/2}\right\}, \tag{4.13}$$

$$\delta N_i = -\frac{N_e^3}{2}\left[p_{31}(\varepsilon_1+\varepsilon_2)+p_{33}\varepsilon_3\right]. \tag{4.14}$$

The experimental results are conveniently analyzed for the parameters $\Delta N_- = \delta N_1 - \delta N_2$ and $\Delta N_+ =$

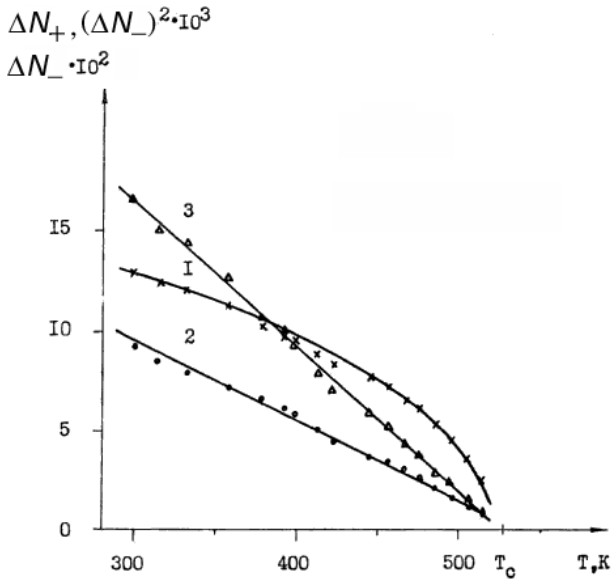

Fig. 15. Temperature dependences of ΔN_- (1), ΔN_+ (2), and $(\Delta N_-)^2$ (3).

$\Delta N_1 + \Delta N_2$. These parameters vary with temperature in the same way as the equilibrium spontaneous strains ε_B and ε_A. The experimental temperature dependences ΔN_- and ΔN_+ are shown in Fig. 15.

The results for ΔN_- correlate with the data of papers [32, 46]. In these papers, the temperature dependences of the birefringence of $BiVO_4$ were studied by the rotating analyzer technique. However, the strain ε_3 with the nonzero equilibrium value was included into expressions (4.13) and (4.14) as opposed to [32]. Thus, the observed temperature dependence of the principal refractive indexes of bismuth vanadate can be explained by the temperature dependence of the spontaneous strain of the crystal with consideration for the elasto-optical effect.

5. Inelastic Light Scattering by Optical and Acoustic Modes

5.1. Raman Scattering in $BiVO_4$

In this section the results of experimental studies by Raman and Brillouin scattering techniques of the lattice dynamics of ferroelastic $BiVO_4$ crystal are presented over a broad temperature range that includes the phase-transition point $T_c = 522$ K. A correlation of the experimental data obtained with the inferences of the phase-transition theory in this crystal is performed.

The techniques of group-theoretical analysis of fundamental vibrations in crystals were employed to establish the selection rules in the Raman spectra. The positional symmetry technique was used [54]. This technique is based on the correlation relations between the symmetry types of vibrations of the space group of free structural units (molecules, ions, atoms, and so on) and the positional symmetry that depends on the position of these particles in the crystal lattice.

Let us perform a group-theoretical analysis of the Raman spectrum for bismuth vanadate at $T > T_c$. In this case, the group C_{4h}^6 is the space symmetry group of the $BiVO_4$ crystal. The point group C_{4h}

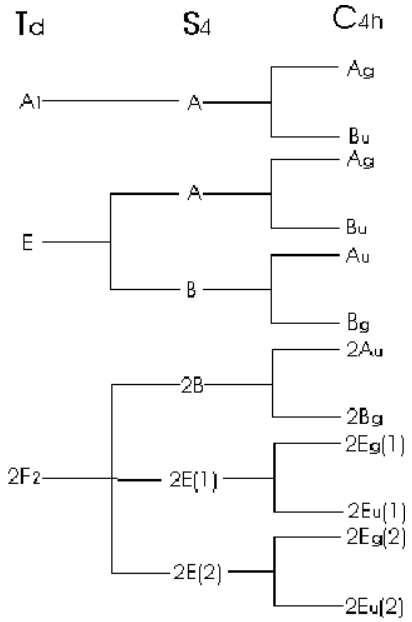

Fig. 16. Correlation diagram of vibrational terms of the VO_4^{3-} ion.

corresponds to it. The unit cell of bismuth vanadate contains two primitive cells. Each of them contains two formula units [26, 41]. Thus, the unit cell contains four bismuth atoms and four vanadium atoms as well as 16 oxygen atoms. In this case, one can distinguish two formula units, a single-particle Bi^{3+} ion and a many-particle VO_4^{3-} ion. It is well known [55] that for such a type of crystals containing p separate particles and m isolated structural groups (many-particle ions) in the primitive cell the full vibrational spectrum includes three acoustic vibrations, $6m + 3p - 3$ external (optical) vibrations ($3m$ of them are orientation vibrations and $3m + 3p - 3$ are translation vibrations), and $3N - 6m - 3p$ internal (optical) vibrations (N is the number of atoms in the primitive cell). Thus, the full vibrational spectrum of $BiVO_4$ should contain 36 vibrations, i.e., 18 internal, 15 external, and 3 acoustic vibrations. Following [54, 56] we determine that S_4 is the space symmetry group for the $BiVO_4$ compound in the paraphase.

We dwell on the analysis of the internal vibrations of the structural group VO_4^{3-}. As is evident from [54] the point group T_d corresponds to ions with the structural formula XY_4. In this case, the optical vibrations are classified by the irreducible representations A_1, E, and $2F_2$. Let us construct the correlation diagram for the internal vibrations of the VO_4^{3-} (see Fig. 16) using the conventional technique presented in [54]. Hence the full representation of the internal vibrations has the form

$$\Gamma_{VO_4^{3-}} = 2A_g + 3B_g + 3A_u + 2B_u + 2E_g + 2E_u.$$

We are coming now to the analysis of the external vibrations of the Bi^{3+} and VO_4^{3-} ions in a $BiVO_4$ crystal. For this purpose the correlation of the symmetry types of the groups S_4 and C_{4h} is performed. Thus the representation of the external vibrations (without regard for acoustic modes) has the form

$$\Gamma_{Bi-VO_4} = A_g + 2B_g + 3E_g + A_u + B_u + 2E_u.$$

According to the selection rules [57] the following types of vibrations should manifest themselves in the Raman spectra of bismuth vanadate at $T > T_c$: $3A_g$, $5B_g$, and $5E_g$. The conditions of manifestation

of the components of the Raman tensor in the spectra at various polarization geometries are defined by the form [54] of this tensor:

$$\mathrm{A}_g \Rightarrow \begin{pmatrix} a & 0 & 0 \\ 0 & a & 0 \\ 0 & 0 & b \end{pmatrix}, \quad \mathrm{B}_g \Rightarrow \begin{pmatrix} c & d & 0 \\ d & -c & 0 \\ 0 & 0 & 0 \end{pmatrix},$$

$$\mathrm{E}_g(1) \Rightarrow \begin{pmatrix} 0 & 0 & e \\ 0 & 0 & f \\ e & f & 0 \end{pmatrix}, \quad \mathrm{E}_g(2) \Rightarrow \begin{pmatrix} 0 & 0 & f \\ 0 & 0 & e \\ -f & e & 0 \end{pmatrix}.$$

In a similar way the Raman spectrum of bismuth vanadate at $T < T_c$ (C_{2h} group) is analyzed. In this case, we obtain for the internal vibrations of VO_4^{3-}

$$\Gamma_{\mathrm{VO}_4^{3-}} = 5A_g + 5A_u + 4B_g + 4B_u.$$

Accordingly, for the external vibrations of (Bi^{3+}–VO_4^{3-}) we have without regard for the acoustic modes

$$\Gamma_{\mathrm{Bi}^{3+}-\mathrm{VO}_4^{3-}} = 3A_g + 6B_g + 2A_u + 4B_u.$$

The full vibrational representation with consideration for the acoustic modes ($\Gamma_{\mathrm{ac}} = A_u + 2B_u$) has the form

$$\Gamma = 8A_g + 10B_g + 8A_u + 10B_u.$$

The corresponding matrices of the Raman tensor are as follows:

$$\mathrm{A}_g \Rightarrow \begin{pmatrix} a & d & 0 \\ d & b & 0 \\ 0 & 0 & c \end{pmatrix}, \quad \mathrm{B}_g \Rightarrow \begin{pmatrix} 0 & 0 & e \\ 0 & 0 & f \\ e & f & 0 \end{pmatrix}.$$

Thus, we carried out the group-theoretical analysis of the Raman spectra of bismuth vanadate for both phase states. It was found that in the Raman spectrum of bismuth vanadate can be observed 18 vibrations in the low-symmetry phase (eight of symmetry A_g and 10 of symmetry B_g) and 13 vibrations in the paraphase (three of symmetry A_g, five of symmetry B_g, and five of symmetry E_g).

The experimental studies of the Raman spectra in BiVO_4 were carried out on the set-up with the parameters given in [58]. Figure 17 presents the Raman spectra of bismuth vanadate of A_g and B_g symmetry types taken at $T = 300$ K for various polarization geometries. The frequencies of the peaks observed and their assignment by the symmetry types are presented in Table 1.

Figures 18a and 18b show the Raman spectra of bismuth vanadate taken at various temperatures. As is seen from Fig. 18, the high-Q soft mode manifests itself in the Raman spectra. Its frequency decreases anomalously at $T \to T_c$. Figure 19 illustrates the temperature dependences of the frequencies of a sequence of optical vibrations. The latter include the soft mode and are related to the B_g type in the paraphase. The studies were carried out in the temperature range 300–600 K.

The free VO_4^{3-} ion is characterized by the T_d group and has four normal vibrations with frequencies 345 (E), 480 (F_2), 825 (F_2), and 870 cm^{-1} (A_1). Three of them are degenerate vibrations.

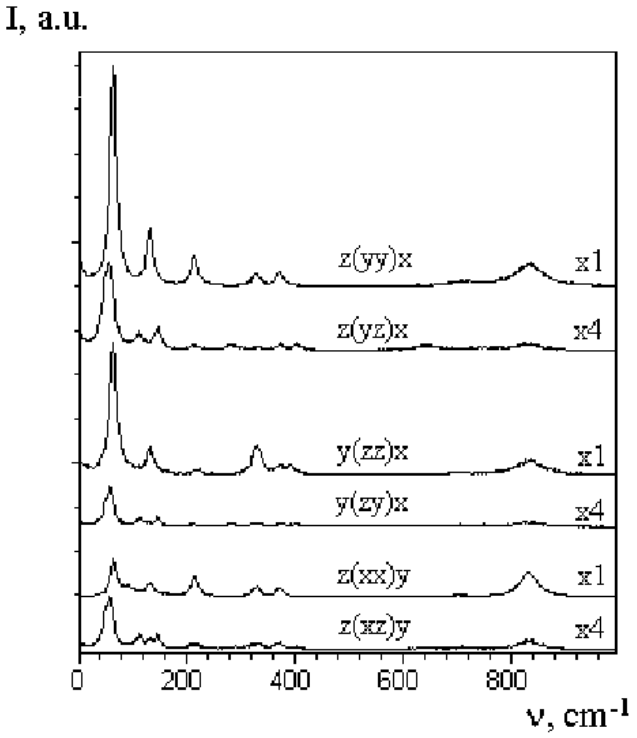

Fig. 17. Raman spectra of the $BiVO_4$ crystal in various scattering geometries at $T = 300$ K.

TABLE 1. Frequencies of the Raman Lines Observed in Bismuth Vanadate and Their Assignment by Symmetry Types.

Type	Frequencies of external vibrations, cm^{-1}	Frequencies of internal vibrations, cm^{-1}
A_g	62, 130, 212	326, 370, 386, 711, 830
B_g	47, 55, 110, 144, 280	400, 642, 743

We managed to observe only six Raman bands from 13 possible combination lines at temperatures above $T_c = 522$ K (see Figs. 19 and 20). This is due to a decrease in the Raman intensity because of an increase in absorption in the crystal with temperature. The Raman spectra corresponding to four polarization states, HH(XX, YY) and HV(XZ, YZ), were studied at $T > T_c$. The Raman bands with frequencies of 48 and 126 cm^{-1} were assigned to vibrations with symmetry E_g, since they were observed for both phases. The line at 25 cm^{-1} (soft mode) should be assigned to the B_g symmetry type above T_c. Below T_c the soft mode is related to the A_g symmetry type, since this mode specifies the symmetry of the low-temperature phase (see Fig. 18).

Let us analyze the temperature dependences of the Raman frequencies of $BiVO_4$ within the framework of the two-oscillator model discussed above. The root-mean-square value of the normal coordinate Q of

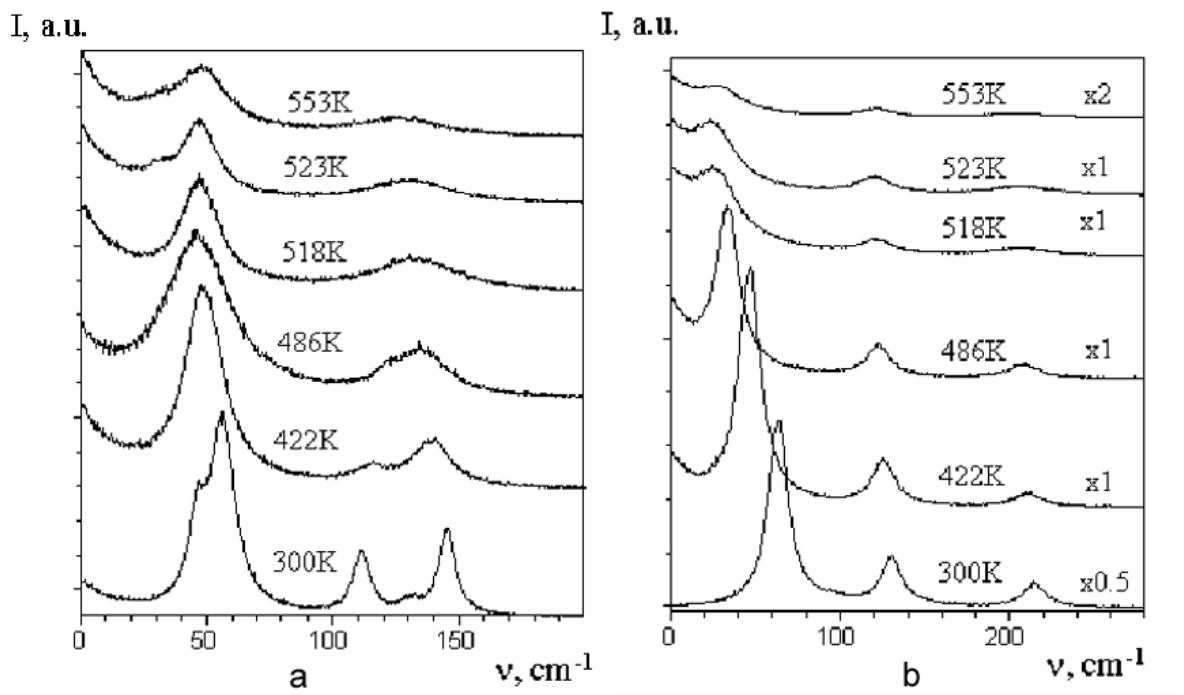

Fig. 18. Raman spectra of the $BiVO_4$ crystal in the scattering geometries $Z(YZ)X$ (a) and $Z(YY)X$ (b).

the soft mode classified as the B_g symmetry type of the initial group C_{4h} is the order parameter for this model. In this case, the crystal symmetry admits the linear in Q interaction of the order parameter and the elastic strain ε_B (the components of the elastic strain ε_B are transformed in the same manner as the order parameter) as well as the quadratic in Q interaction between the order parameter and the elastic strain ε_A. The latter interaction is associated with the full-symmetric representation A_g of the initial symmetry group of the crystal.

Let us rewrite the thermodynamic potential (2.14) to include the terms corresponding to these interactions,

$$F - F_0 = \underbrace{\frac{1}{2}A(T-T_0)Q^2 + \frac{1}{4}BQ^2}_{\Delta F_{\rm opt}} + \underbrace{\frac{1}{2}c_B\varepsilon_B^2 + \frac{1}{2}c_A\varepsilon_A^2}_{\Delta F_{\rm ac}} + \underbrace{k_A\varepsilon_A Q^2 + k_B\varepsilon_B Q}_{\Delta F_{\rm int}}$$

$$+\frac{1}{2}m_E\omega_E^2(E_1^2+E_2^2) + \frac{1}{2}a_1Q(E_1^2-E_2^2) + b_1QE_1E_2 + \frac{1}{2}m_A\omega_A^2A^2 + M_AAQ^2. \qquad (5.1)$$

Here, $\Delta F_{\rm opt}$ is the contribution of the optical mode of the B_g symmetry type, $\Delta F_{\rm ac}$ is the contribution of the acoustic modes of the symmetries A_g and B_g, $\Delta F_{\rm int}$ are terms that include the contributions of the other modes, k_A, k_B, a_1, b_1, and M_A are the coupling constants, and A and E_i are the normal coordinates of the A_g and E_g modes.

Using the equilibrium conditions in the Landau theory of phase transitions, we obtain from expression (5.1) the temperature dependences of the frequencies of optical vibrations renormalized because of

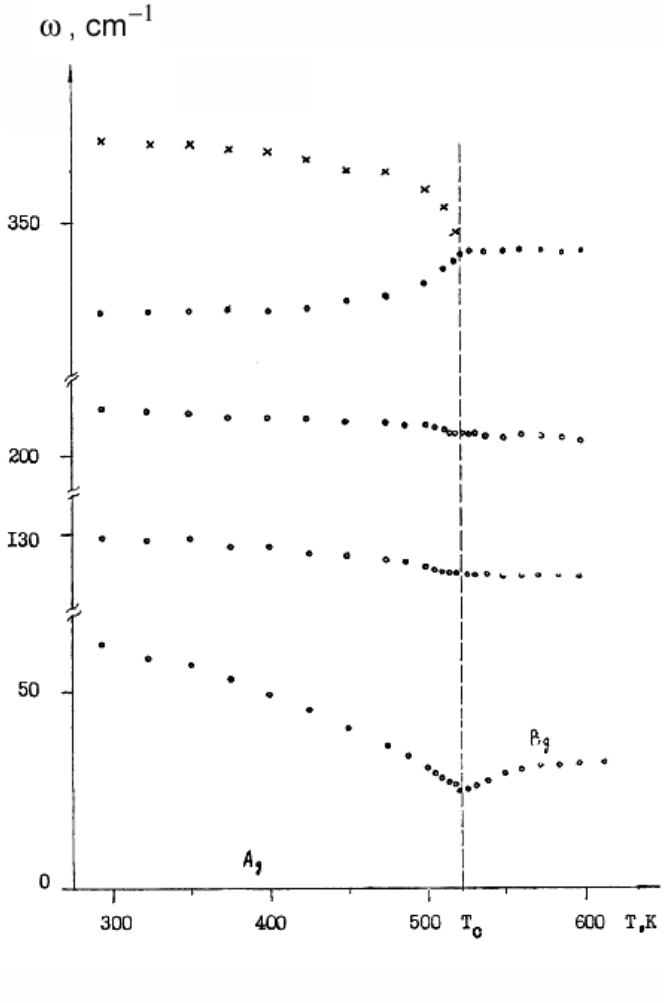

Fig. 19. Temperature dependences of the frequencies of several Raman lines of the A_g type at $T < T_c$.

interaction. In this case, we have for the vibration corresponding to the soft mode

$$\omega_Q^2 = \begin{cases} A_0(T - T_0) & \text{with} \quad T \geq T_c, \\ A_0'(T_0' - T) & \text{with} \quad T < T_c, \end{cases} \tag{5.2}$$

where

$$A_0' = A_0 \frac{2}{1 - x'} , \quad T_0' = T_0 + \frac{1 - x'}{2}(T_c - T_0).$$

For the mode of the E_g type the following relationships hold true:

$$\omega_{E_{1,2}} = \begin{cases} \omega_{0E}^2 & \text{with} \quad T \geq T_c, \\ \omega_{0E}^2 \pm \sqrt{a_1^2 + b_1^2 Q_0} & \text{with} \quad T < T_c. \end{cases} \tag{5.3}$$

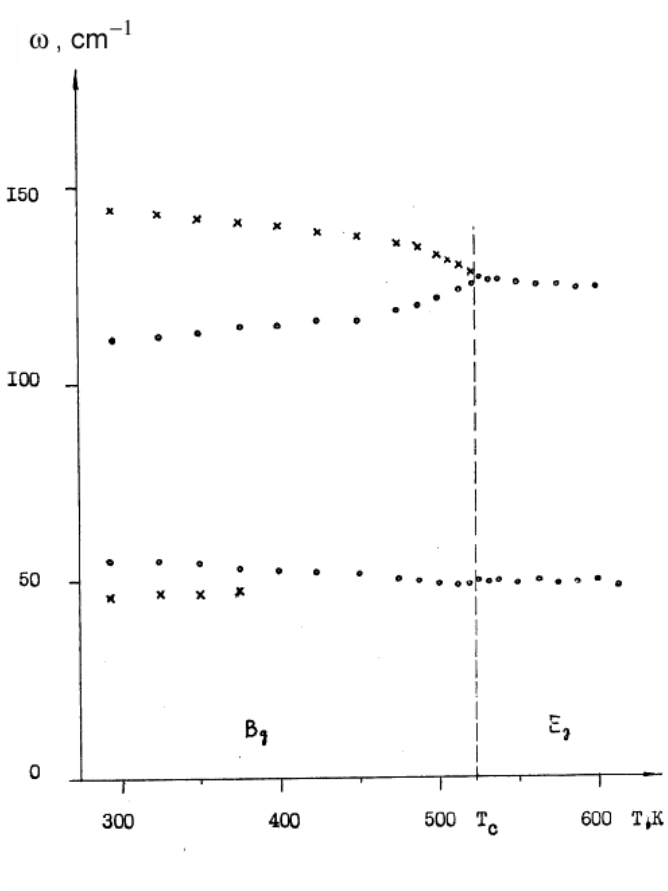

Fig. 20. Temperature dependences of the frequencies of the Raman bands of the B_g type at $T < T_c$.

Correspondingly for the A_g mode we obtain

$$\omega_A = \begin{cases} \omega_{0A}^2 & \text{with} \quad T \geq T_c, \\ \omega_{0A}^2 - \dfrac{4M_A Q_0^2}{A(T-T_0) - (3-x')BQ_0^2} & \text{with} \quad T < T_c, \end{cases} \tag{5.4}$$

where

$$Q_0^2 = \begin{cases} 0 & \text{with} \quad T \geq T_c, \\ \dfrac{A_0(T_c - T)}{B(1-x')} & \text{with} \quad T < T_c, \end{cases}$$

$$T_c = T_0 + \frac{k_B^2}{A_0 c_B}\,, \quad x' = x + \frac{2M_A^2}{Bm_A}\,, \quad x = \frac{2k_A^2}{BC_A}\,.$$

As is seen from expressions (5.2)–(5.4) and Fig. 21, the interaction of the soft optical mode of the symmetry B_g with the soft acoustic mode of the same symmetry and with the optical modes of the A_g and E_g types results in the violation of the well-known relationship for the Curie–Weiss constants in the paraelastic and ferroelastic phases (the "law of two," see Fig. 21) as well as in the increase in the

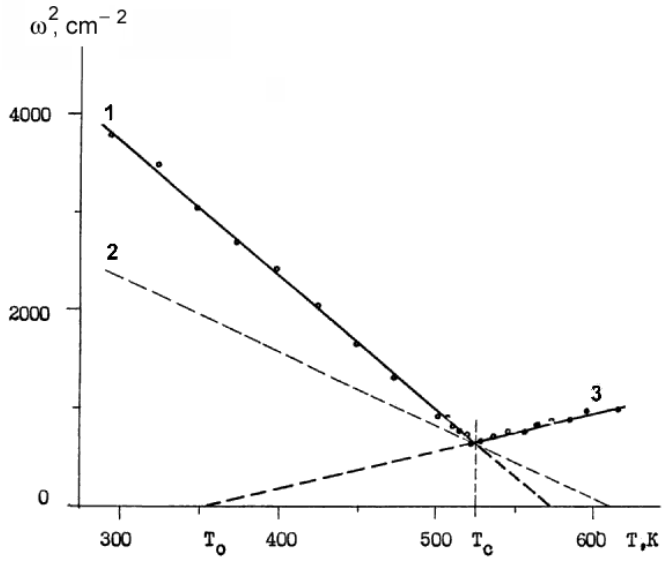

Fig. 21. Temperature dependence of the squared frequency of the soft optical mode. Points are experimental data, while solid lines are theory. The dashed line 2 corresponds to the "law of two."

temperature of phase transition from T_0 up to T_c. The temperature behavior of the frequencies of all the lattice modes observed can be explained by their strong dependence on the order parameter.

The treatment of the experimental dependences of Raman frequencies by formulas (5.2)–(5.4) results in the following parameters of the interacting oscillators:

$$A_0 = 4.6 \pm 0.3 \text{ cm}^{-2}/\text{K}, \quad A_0' = 13.3 \pm 0.1 \text{ cm}^{-2}/\text{K},; \quad x' = 0.31 \pm 0.04,$$

$$T_c = 522 \text{ K}, \quad T_0 = 330 \pm 20 \text{ K}, \quad T_0' = 588 \pm 10 \text{ K},$$

$$C_A = 9.5 \cdot 10^{10} \text{ Pa}, \quad C_B = 3.7 \cdot 10^{10} \text{ Pa},$$

$$\omega_{E1} = 126.3 \pm 0.5 \text{ cm}^{-1}, \quad \omega_{E2} = 49.4 \pm 0.5 \text{ cm}^{-1}, \quad \omega_A = 326.9 \pm 0.5 \text{ cm}^{-1}.$$

The theoretical dependences (5.2)–(5.4) constructed using these parameters are shown by the solid lines in Fig. 21.

5.2. Brillouin Scattering in $BiVO_4$

The theory of elasticity as well as the theory of propagation of acoustic bulk waves in a linear anisotropic medium are well developed at present [59–63]. The small strain of the continuous medium is generally described by the distortion tensor with the components $\gamma_{ik} = \partial u_i/\partial x_k$, where $\vec{u}$ is the translation vector and x_k is the coordinate. The distortion tensor can be resolved into the symmetric component

$$u_{ik} = \frac{1}{2}\left(\frac{\partial u_i}{\partial x_k} + \frac{\partial u_k}{\partial x_i}\right) \tag{5.5}$$

referred to as the tensor of small strains and the antisymmetric component

$$\omega_{ik} = \frac{1}{2}\left(\frac{\partial u_i}{\partial x_k} - \frac{\partial u_k}{\partial x_i}\right) \tag{5.6}$$

designated as the tensor of small rotations. The relation between the strain tensor (and in the general case the distortion tensor) and the stress tensor σ_{ij} is determined by the generalized linear Hooke's law. Without considering the temperature expansion, the latter has the form

$$\sigma_{ij} = C_{ijkl}u_{kl}, \tag{5.7}$$

where C_{ijkl} is the material fourth-rank tensor referred to as the tensor of elastic coefficients. The components of this tensor are also designated as the modulus of elasticity or elastic constants. Let us substitute (5.7) into the equation of motion for a volume element of the solid (Cauchy equation). We have

$$\frac{\partial \sigma_{ik}}{\partial x_k} = \rho \frac{\partial^2 u_i}{\partial t^2}\ , \tag{5.8}$$

where ρ is the density of the body. This results in the elastodynamic equation in the form

$$C_{ijkl}\frac{\partial^2 u_k}{\partial x_j \partial x_l} = \rho \frac{\partial^2 u_i}{\partial t^2}\ . \tag{5.9}$$

The plane harmonic elastic wave in the medium is described by the field of the translation vector

$$\vec{u}(\vec{r}, t) = A\vec{\gamma}\exp i(\vec{k}\vec{r} - \omega t), \tag{5.10}$$

where A is the wave amplitude, $\vec{\gamma}$ is the unit vector of polarization, $\vec{k} = \frac{2\pi}{\lambda}\vec{\chi}$ is the wave vector, and $\vec{\chi}$ is the unit vector of the wave normal. Substituting (5.10) into (5.9) and differentiating we obtain the Christoffel equation

$$C_{ijkl}\chi_j\chi_k\chi_l = \rho v^2\gamma_i, \tag{5.11}$$

or (in matrix form) the Green–Christoffel equation

$$|\Gamma_{ik} - \rho v^2\delta_{ik}|\gamma_k = 0. \tag{5.12}$$

Here, $\Gamma_{ik} = C_{ijkl}\chi_j\chi_i$ is the Christoffel tensor, v is the phase velocity of the wave, δ_{ik} is the Kronecker symbol, and γ_i is the unit vector of polarization, which satisfies the condition $\gamma_i\gamma_i = 1$.

Thus, with known elastic constant matrix C_{ijkl} one can determine the phase velocities v_n and polarizations γ_i of three elastic waves propagating along the specified direction $\vec{\chi}$ in the crystal from the solution of the eigenvalue and eigenvector problem.

The inverse problem, the determination of the C_{ijkl} matrix from the experimental velocities of the elastic waves, presents more difficulties. In the case where the C_{ijkl} matrix has N independent components from the symmetry conditions, one has to select such crystallographic directions in the crystal that provide the possibility of determining the velocities of N different nonequivalent waves. The system of N nonlinear equations $v_n = f_n(C_{ijkl})$ is constructed on the basis of the measured data, whose solution gives the desired values C_{ijkl}. In this case, the selection of these directions in the crystal should be such that the elastic constants C_{ijkl} in the expressions for the velocities v_n to be determined enter in combinations that provide the possibility of determining not only the modulus but also the sign of each constant C_{ijkl}.

The solution of the direct elastic problem (5.12), i.e., finding the acoustic wave velocity along the specified direction χ_i with known elastic constant matrix C_{ijkl}, is reduced to the solution of the corresponding characteristic equation (5.12). The accuracy of calculation of v_i should be determined by the accuracy of determination of the direction χ_i and of C_{ijkl}. In this case, the error in determining v_i is a complex nonlinear function of the errors in determining C_{ijkl}.

In the general case the problem of finding n independent elastic constants of a crystal from a set of k experimental velocities of elastic waves for k independent directions is reduced to the solution of a system of k nonlinear equations

$$F_i(\{C\}) = 0, \quad i = 1, 2, \ldots k \geq n. \tag{5.13}$$

Here, f_i is a characteristic polynomial whose argument is the ith experimental velocity, while its coefficients are known functions of n independent elastic constants of the crystal. These functions are independent and to be determined when solving system (5.13).

It should be noted that system (5.13) can be solved in the analytic form only for high-symmetry crystals in the case where the set of velocities $\{v\}$ is determined for the directions chosen by the symmetry. However, for monoclinic crystals the problem is reduced to the solution of a system of 12 nonlinear equations and can be solved only by numerical techniques.

With $k = n$ the problem is a purely algebraic one. In this case, the solution depends on the choice of experimental data $\{v\}$, and accidental measurement errors can strongly affect the result. In the case of linear system (5.13) it is solved by the least-squares technique. There are no optimal estimation methods in nonlinear problems. However, a solution can be obtained on the basis of the maximum likelihood method. The realization of the latter is based on the various ways of linearization of the problems with subsequent using of the least-squares technique [64–68].

We have created a program for solving the elasticity theory problem [69]. In this program the standard subroutine of minimization of the sum of squares of the MINQ function according to the method of the steepest descent is used. The operation of this program was repeatedly proved by the example of calculating the elastic constants of α-quartz with alternate solution of both the inverse and direct problems. In this case, various arrays C_{ijkl} were preset as an initial estimate and the program was tested with various preset spreads of v_i. Tests revealed the high reliability and efficiency of the program.

The temperature studies of the acoustic properties of bismuth vanadate were carried out with the technique [70, 71] of analysis of the spectra of Brillouin scattering. Information on the lattice transformation with temperature is contained in the frequency shifts of the components of Brillouin scattering and in the variation in their intensity. The relationship

$$v = \frac{\Omega\lambda}{2\pi\sqrt{n_i^2 + n_s^2}} \tag{5.14}$$

was used to find the velocities v of the elastic waves. Here, λ is the wavelength of incident light, n_i and n_s are the refractive indexes of the crystal determined by the polarization of incident and scattered light, and Ω is the acoustic phonon frequency.

The intensity of light scattering by acoustic phonons in the crystal is determined up to a geometrical factor by the following expression:

$$I \sim \frac{(P_{ijkl} d_i d_j \chi_k \gamma_l)^2}{\rho v^2} n_i^2 n_s^2. \tag{5.15}$$

Here, n_i and n_s are the refractive indexes of the crystal, v is the acoustic wave velocity, ρ is the crystal density along the direction of acoustic wave propagation, P_{ijkl} is the effective value of the elasto-optical

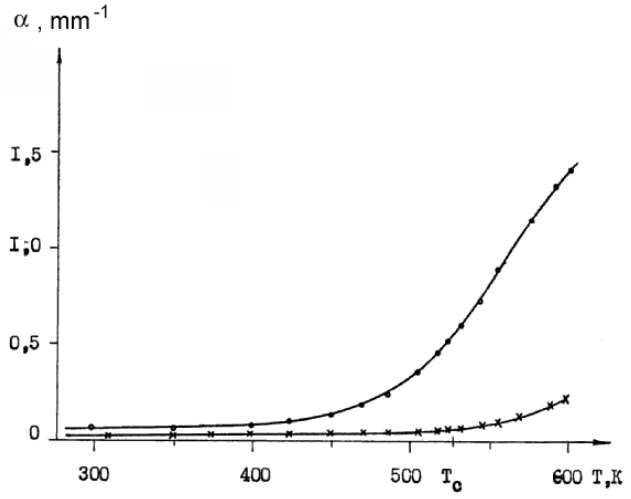

Fig. 22. Temperature dependences of the absorption coefficients in the $BiVO_4$ crystal with HH (upper curve) and VV polarizations of the incident and scattered light.

modulus, and χ and γ are unit vectors along the directions of propagation and polarization of the elastic wave.

The results of Raman studies of $BiVO_4$ bear witness to the "softening" of the optical phonon of symmetry B_g in the paraphase. This results in the strong coupling of this vibration with acoustic modes of the B_g type of symmetry and eventually in their strong temperature dependence [31]. For experimental verification of this assumption we studied several types of acoustic modes of $BiVO_4$ crystal using the Brillouin scattering technique [69, 70]. The temperature dependences of combinations of the elastic moduli corresponding to the A_g and B_g symmetry types were determined [69].

The temperature dependences of the components of Brillouin scattering for 14 acoustic waves within the temperature range 300–550 K were studied using an automated Brillouin scattering spectrometer [71]. The temperature dependence of the absorption coefficient should be taken into account when determining the variations in the intensity of the components of Brillouin scattering, since $BiVO_4$ crystals possess strong light absorption at high temperatures. For this purpose the intensity of laser radiation before the sample (J_0) and after it (J_1) was measured. The absorption coefficient α was determined from the expression $J_1 = J_0 \exp(-\alpha l)$, where l is the distance traveled by light in the crystal. The temperature dependences of the absorption coefficients for HH (the electric-field vector of the incident light wave is parallel to the crystal symmetry axis) and VV (the electric-field vector of the incident light wave is perpendicular to the crystal symmetry axis) polarizations of the incident and scattered light are presented in Fig. 22.

The spectra of Brillouin scattering by the acoustic soft mode at various temperatures are shown in Fig. 23. The temperature variations in this mode (frequency shift and variation in the intensity of Brillouin scattering) are well pronounced here.

The temperature dependences of the frequency of the soft acoustic mode in $BiVO_4$ were obtained on the basis of these measurements (see Fig. 24). The corresponding calculated values of the critical elastic modulus $C_c(T)$ are presented in Fig. 25.

Four bismuth vanadate samples with the corresponding orientations were used to find the full elastic

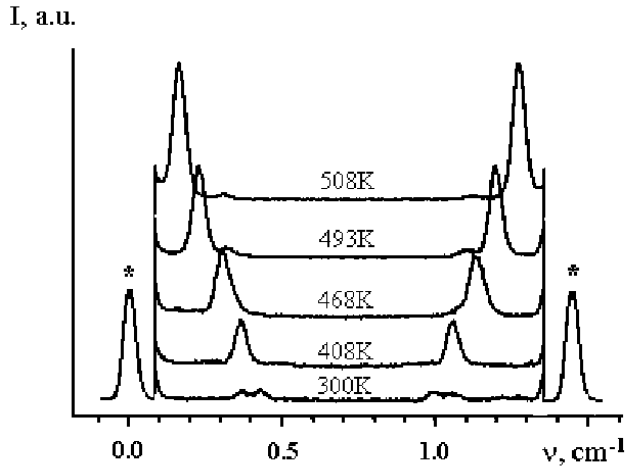

Fig. 23. Spectra of Brillouin scattering by the acoustic soft mode in bismuth vanadate. The central maxima of the neighboring orders of interference are marked off by asterisks.

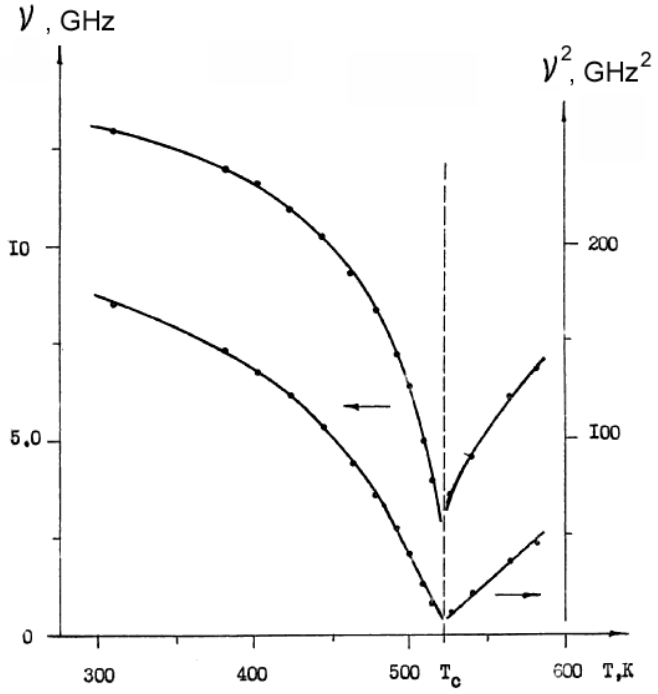

Fig. 24. Temperature dependences of the frequency of the soft acoustic mode of $BiVO_4$ and its square.

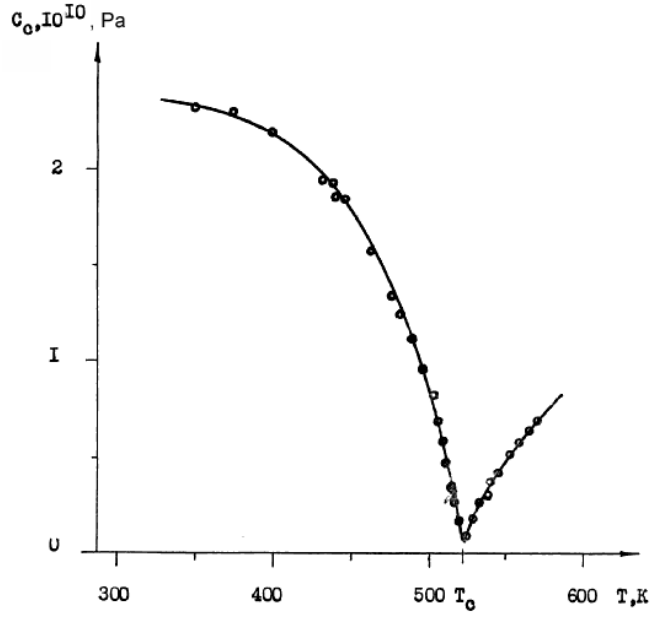

Fig. 25. Temperature dependence of the critical elastic modulus $C_c(T)$.

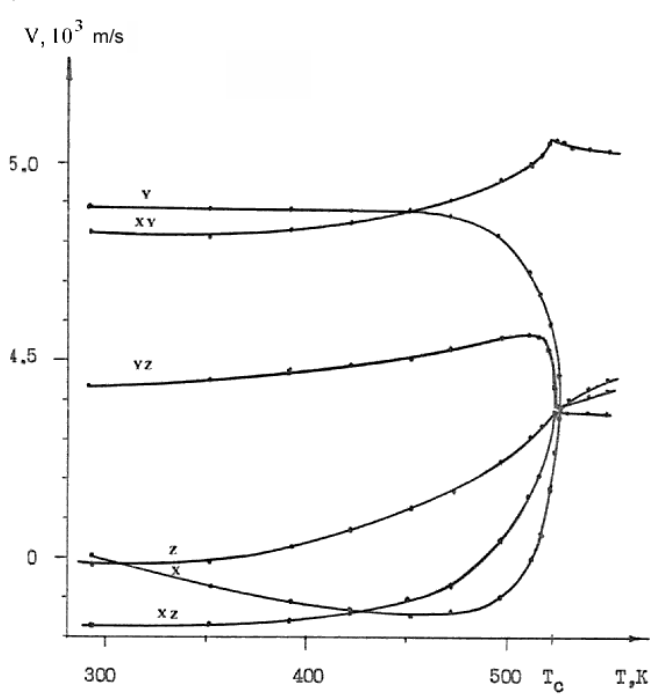

Fig. 26. Temperature dependence of the velocities of acoustic waves along different directions in $BiVO_4$ crystals within the range 3.6–5.2 m/s.

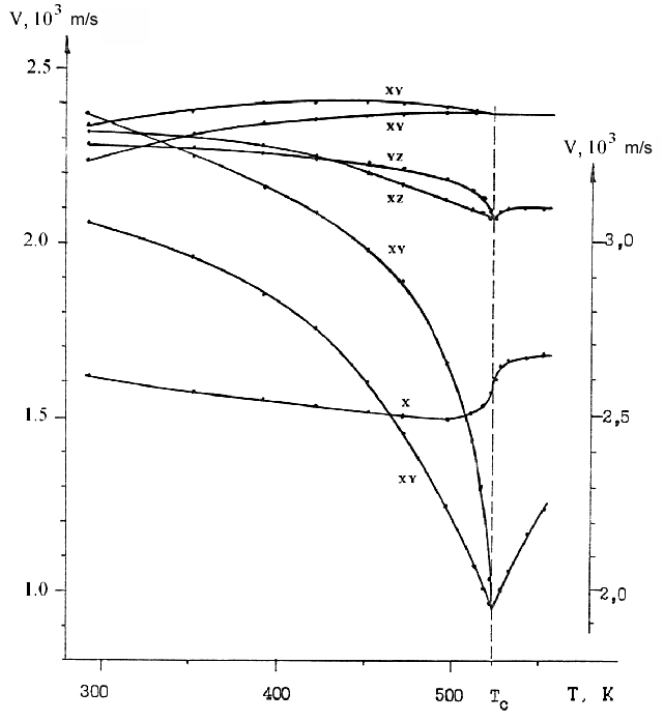

Fig. 27. Temperature dependence of the velocities of acoustic waves along different directions in $BiVO_4$ crystals within the range 1–2.5 m/s.

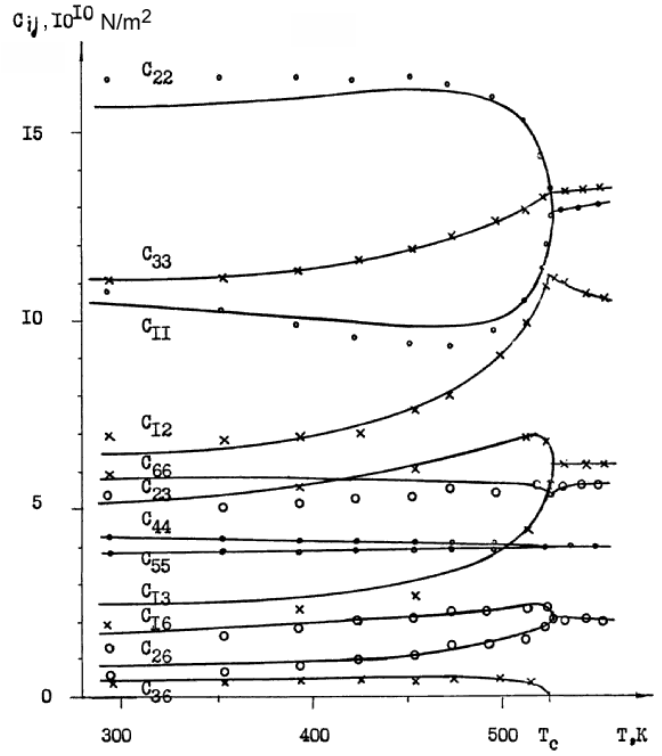

Fig. 28. Temperature dependence of the elastic moduli in $BiVO_4$ crystals.

modulus matrix. For these samples we determined 14 frequencies of the components of Brillouin scattering for 14 various nonequivalent acoustic waves of the crystal at different fixed temperatures. The velocities of the acoustic waves were determined with expression (5.14). The refractive indexes obtained in [53] were used in the calculations of the velocities. The results of these calculations can be seen in Figs. 26 and 27.

The full elastic constant matrix of a crystal was found for each temperature with the technique described above using the temperature dependences of the velocities of 14 elastic waves. For this purpose the developed program optimized the coefficients of the parent matrix to minimize the sum of the squared deviations of the experimental and calculated velocities for all waves. The calculation procedure for the elastic constants, orientation of the bismuth vanadate crystals, and, correspondingly, the directions of propagation of the acoustic waves were the same as in [72]. The temperature dependences of the principal refractive indexes of $BiVO_4$ [53] were taken into account in the calculations of the sound velocities. The temperature dependences of the velocities of acoustic waves are shown in Figs. 26 and 27, and the corresponding dependences of the coefficients $C_{ij}(T)$ are shown in Figs. 25 and 28.

To calculate the theoretical dependences $C_{ij}(T)$ we use according to [33] the expansion of the crystal free energy in terms of the order parameter Q [see (2.14)]. In this case, we take into account in (2.14) all the contributions of the optical and acoustic soft phonons to the free energy as well as terms that describe the coupling of the optical soft mode with acoustic modes of the A_g and B_g symmetries. We have

$$\begin{aligned}\Delta F &= \frac{1}{2}A(T-T_0)Q^2+\frac{1}{4}BQ^2+[k_B\alpha(\varepsilon_1-\varepsilon_2)+k_B\beta\varepsilon_6]Q\\ &+[k_A(\varepsilon_1+\varepsilon_2)+k_A\varepsilon_3]Q^2+\frac{1}{2}K_3(\varepsilon_4-\varepsilon_5)Q+K_4\varepsilon_4\varepsilon_5Q\\ &+\frac{1}{2}C^0_{11}(\varepsilon_1^2+\varepsilon_2^2)+C^0_{12}\varepsilon_1\varepsilon_2+C^0_{13}\varepsilon_1\varepsilon_3+C^0_{23}\varepsilon_2\varepsilon_3+\frac{1}{2}C^0_{33}\varepsilon_3^2\\ &+\frac{1}{2}C^0_{gg}\varepsilon_6^2+C^0_{16}(\varepsilon_1-\varepsilon_2)\varepsilon_6+\frac{1}{2}C^0_{44}(\varepsilon_4^2+\varepsilon_5^2).\end{aligned} \tag{5.16}$$

Note that the asymptotic elastic moduli C^0_{ij} are used in the terms corresponding to the elastic crystal energy in expression (5.16) for $T \gg T_0$.

To calculate the temperature dependences of the elastic moduli we use the relationship [73]

$$C_{ik}=\left(\frac{\partial^2 F}{\partial\varepsilon_i\varepsilon_k}\right)_Q-\frac{\dfrac{\partial^2 F}{\partial\varepsilon_i\partial Q}\cdot\dfrac{\partial^2 F}{\partial Q\partial\varepsilon_k}}{\dfrac{\partial^2 F}{\partial Q^2}}\,. \tag{5.17}$$

For the temperature dependences $C_{\alpha\beta}(\Delta T)$ ($\Delta T = T_c - T$) we obtain for the ferroelectric phase at $T < T_c$

$$\begin{aligned}C_{11} &= C^0_{11}-\frac{M_2\Delta T+2\sqrt{\alpha^2C^0_BM_1M_2\Delta T}+\alpha^2C^0_BM_1}{\Delta T+M_1}\\ &= \bar{C}_{11}-\frac{2\sqrt{\alpha^2C^0_BM_1M_2\Delta T}+(M_2-\alpha^2C^0_B)\Delta T}{\Delta T+M_1}\,,\end{aligned} \tag{5.18}$$

$$\begin{aligned} C_{22} &= C_{22}^0 - \frac{M_2\Delta T - 2\sqrt{\alpha^2 C_B^0 M_1 M_2 \Delta T} + \alpha^2 C_B^0 M_1}{\Delta T + M_1} \\ &= \bar{C}_{11} + \frac{2\sqrt{\alpha^2 C_B^0 M_1 M_2 \Delta T} - (M_2 - \alpha^2 C_B^0)\Delta T}{\Delta T + M_1}\,, \end{aligned} \tag{5.19}$$

$$C_{12} = C_{12}^0 - \frac{M_2\Delta T - \alpha^2 C_B^0 M_1}{\Delta T + M_1} = \bar{C}_{12} - \frac{(M_2 + \alpha^2 C_B^0)\Delta T}{\Delta T + M_1}\,, \tag{5.20}$$

$$C_{66} = C_{66}^0 - \frac{\beta^2 C_B^0 M_1}{\Delta T + M_1} = \bar{C}_{66} + \frac{\beta^2 C_B^0 \Delta T}{\Delta T + M_1}\,, \tag{5.21}$$

$$C_{16} = C_{16}^0 - \frac{\sqrt{\beta^2 C_B^0 M_1 M_2 \Delta T} + \alpha\beta C_B^0 M_1}{\Delta T + M_1} = \bar{C}_{16} - \frac{\alpha\beta C_B^0 \Delta T - \sqrt{\beta^2 C_B^0 M_1 M_2 \Delta T}}{\Delta T + M_1}\,, \tag{5.22}$$

$$C_{26} = C_{26}^0 - \frac{\sqrt{\beta^2 C_B^0 M_1 M_2 \Delta T} - \alpha\beta C_B^0 M_1}{\Delta T + M_1} = \bar{C}_{16} - \frac{\alpha\beta C_B^0 \Delta T + \sqrt{\beta^2 C_B^0 M_1 M_2 \Delta T}}{\Delta T + M_1}\,, \tag{5.23}$$

$$C_{33} = C_{33}^0 - \frac{M_2\Delta T}{\Delta T + M_1} = \bar{C}_{33} - \frac{M_2\Delta T}{\Delta T + M_1}\,, \tag{5.24}$$

$$C_{13} = C_{13}^0 - \frac{M_2\Delta T + 2\sqrt{\alpha^2 C_B^0 M_1 M_2 \Delta T}}{\Delta T + M_1} = \bar{C}_{13} - \frac{M_2\Delta T + 2\sqrt{\alpha^2 C_B^0 M_1 M_2 \Delta T}}{\Delta T + M_1}\,, \tag{5.25}$$

$$\begin{aligned} C_{23} &= C_{23}^0 - \frac{M_2\Delta T - 2\sqrt{\alpha^2 C_B^0 M_1 M_2 \Delta T}}{\Delta T + M_1} = \bar{C}_{23} - \frac{M_2\Delta T - 2\sqrt{\alpha^2 C_B^0 M_1 M_2 \Delta T}}{\Delta T + M_1}\,, \\ C_{36} &= C_{36}^0. \end{aligned} \tag{5.26}$$

The temperature dependences $C_{\alpha\beta}(\Delta T)$ at $T > T_c$ are the following:

$$C_{11} = C_{22} = C_{11}^0 - \alpha^2 C_B^0 \frac{T_c - T_0}{T - T_0} = \bar{C}_{11} + \alpha^2 C_B^0 \frac{T - T_c}{T - T_0}\,, \tag{5.27}$$

$$C_{12} = C_{12}^0 + \alpha^2 C_B^0 \frac{T_c - T_0}{T - T_0} = \bar{C}_{12} - \alpha^2 C_B^0 \frac{T - T_c}{T - T_0}\,, \tag{5.28}$$

$$C_{66} = C_{66}^0 - \beta^2 C_B^0 \frac{T_c - T_0}{T - T_0} = \bar{C}_{66} - \beta^2 C_B^0 \frac{T - T_c}{T - T_0}\,, \tag{5.29}$$

$$C_{16} = C_{16}^0 - \alpha\beta C_B^0 \frac{T_c - T_0}{T - T_0} = \bar{C}_{16} + \alpha\beta C_B^0 \frac{T - T_c}{T - T_0}\,, \tag{5.30}$$

$$C_{26} = C_{26}^0 + \alpha\beta C_B^0 \frac{T_c - T_0}{T - T_0} = \bar{C}_{26} - \alpha\beta C_B^0 \frac{T - T_c}{T - T_0}\,, \tag{5.31}$$

$$C_{33} = C_{33}^0 = \bar{C}_{33}, \quad C_{13} = C_{13}^0 = \bar{C}_{13}. \tag{5.32}$$

As is seen from expressions (5.18)–(5.32), the temperature dependences of all the elastic moduli can be expressed in terms of the values of these constants at the phase transition point $\bar{C}_{\alpha\beta}(T = T_c)$ as well as of the six parameters

$$M_1 = \frac{(1-x)}{2}(T_c - T_0), \quad M_2 = xC_A^0, \quad C_B^0, \quad \alpha, \quad \beta, \quad \text{and} \quad T_0.$$

The exception are the elastic constants C_{44}, C_{55}, and C_{45}. Their temperature dependence is weak because of the weakness of interaction of their associated acoustic modes with the order parameter.

Considering these six parameters as the fitting ones and using the experimental values of $\bar{C}_{\alpha\beta}(T = T_c)$, we determine their values that provided the best agreement of the experimental values of $C_{\alpha\beta}(T)$ with theoretical curves (5.18)–(5.32) (see Fig. 28). These values are the following: $M_1 = 69$ K, $M_2 = 2.9 \cdot 10^{10}$ Pa, $C_B^0 = 3.7 \cdot 10^{10}$ Pa, $\alpha = 0.943$, $\beta = 0.332$, and $T_0 = 330$ K.

Using the values of M_1, M_2, and T_0, we find that $x = 0.303$ and $C_A^0 = 9.5 \cdot 10^{10}$ Pa. These values agree well with those found previously [25, 29].

For combinations of the elastic moduli of symmetry A_g, we have

$$\frac{1}{2}(C_{11} + C_{12}) = \frac{1}{2}(C_{11}^0 + C_{12}^0) - (4k_A^2Q^2 + 2\alpha k_A k_B Q)\Psi, \tag{5.33}$$

$$\frac{1}{2}(C_{22} + C_{12}) = \frac{1}{2}(C_{11}^0 + C_{12}^0) - (4k_A^2Q^2 - 2\alpha k_A k_B Q)\Psi, \tag{5.34}$$

$$C_{33} = C_{33}^0 + 4k_A^2Q^2\Psi, \tag{5.35}$$

$$C_{13} = C_{13}^0 - (4k_A^2Q^2 + 2\alpha k_A k_B Q)\Psi, \tag{5.36}$$

$$C_{23} = C_{23}^0 - (4k_A^2Q^2 - 2\alpha k_A k_B Q)\Psi, \tag{5.37}$$

where

$$\Psi = [A_0(T - T_0) + (3 - x)BQ^2]^{-1}. \tag{5.38}$$

For combinations of the elastic moduli of symmetry B_g, we obtain

$$\frac{1}{2}(C_{11} - C_{12}) = \frac{1}{2}(C_{11}^0 - C_{12}^0) - (\alpha^2k_B^2 + 2\alpha k_A k_B Q)\Psi, \tag{5.39}$$

$$\frac{1}{2}(C_{22} - C_{12}) = \frac{1}{2}(C_{11}^0 - C_{12}^0) - (\alpha^2k_B^2 - 2\alpha k_A k_B Q)\Psi, \tag{5.40}$$

$$C_{66} = C_{66}^0 - \beta^2k_B^2\Psi, \tag{5.41}$$

$$C_{16} = C_{16}^0 - (\alpha\beta k_B^2 + 2\beta k_A k_B Q)\Psi, \tag{5.42}$$

$$C_{26} = C_{26}^0 - (\alpha\beta k_B^2 + 2\beta k_A k_B Q)\Psi, \tag{5.43}$$

The dependences obtained are shown in Figs. 29 and 30. As is seen from Fig. 29 there are no variations in the elastic moduli of symmetry A_g at $T > T_c$.

From a comparison of the theoretical dependences (5.33)–(5.43) (shown in Figs. 29 and 30 by the solid lines) with the experimental data, six fitting parameters were determined that provide the minimum discrepancy between theory and experiment throughout the temperature range. The values of these parameters are the following: $C_A = 7.84 \cdot 10^{10}$ Pa, $C_B = 3.7 \cdot 10^{10}$ Pa, $\alpha = 0.943$, $\beta = 0.332$, $T_0 = 330$ K, and $x = 0.37$. Note that the values of the last three parameters agree satisfactorily with those obtained

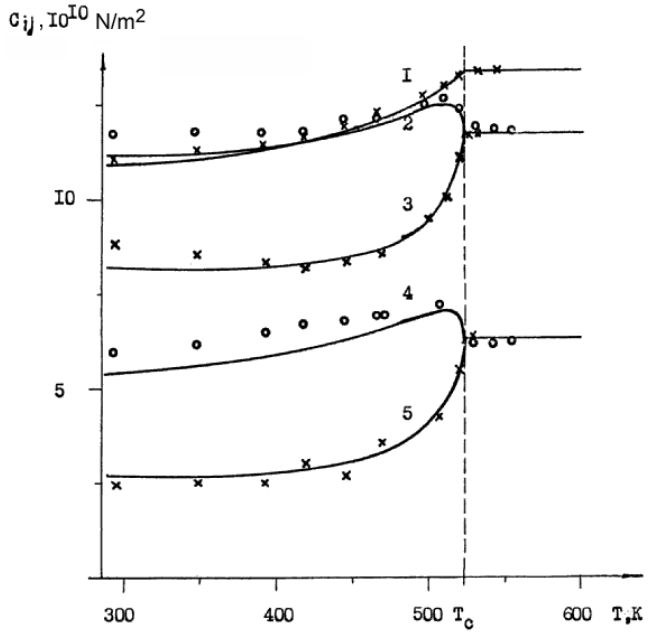

Fig. 29. Temperature dependence of the linear combination of elastic moduli of symmetry A_g for the $BiVO_4$ crystal.

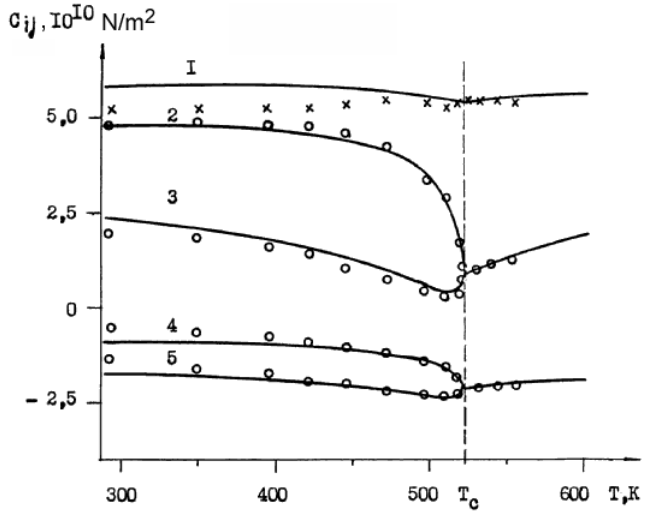

Fig. 30. Temperature dependence of the linear combination of elastic moduli of symmetry B_g for the $BiVO_4$ crystal.

earlier in studies of optical [25] and acoustic [29] soft modes. The calculated moduli have the following values (in units of 10^{10} Pa):

$$\frac{1}{2}(C_{11}^0 - C_{12}^0) = 4.3, \quad \frac{1}{2}(C_{11}^0 + C_{12}^0) = 11.7,$$
$$C_{66}^0 = 5.9, \quad C_{16}^0 = -1.1, \quad C_{33}^0 = 13.3, \quad C_{13}^0 = 6.2.$$

Thus, the temperature dependences of the elastic modulus matrix of bismuth vanadate crystals as well as of the frequencies of the acoustic modes studied can be described within the framework of the Landau theory with consideration for the coupling of the acoustic modes with the optical soft mode of symmetry B_g.

5.3. Intensity of Light Scattering in $BiVO_4$ Crystals by Soft Modes in the Vicinity of the Phase Transition

In considering the kinetics of permittivity fluctuations that defines the spectrum of scattered radiation, one has to consider the contributions of fluctuations of the order parameters and of the acoustic strain, which are linearly related to each other by long-range elastic forces [74]. Using the general theory of light scattering by coupled modes [74–77], we obtain the following expression for the spectral density of the scattered light intensity in the HH polarization (horizontal orientation of the polarizer and analyzer) in terms of the generalized susceptibilities:

$$I_{HH}(\omega) = D\varepsilon_q^4 \operatorname{Im}\sum_{i,j=1}^{2} p_i p_j \chi_{ij} = D\varepsilon_q^4 \frac{kT}{\pi\omega}(p_{qQ}^2 \chi'_{QQ}{}'' + 2p_{qQ}p_{q\varepsilon}\chi''_{Q\varepsilon} + p_{q\varepsilon}^2 \chi''_{\varepsilon\varepsilon}). \tag{5.44}$$

Here, $\varepsilon_q^2 = \varepsilon_{\alpha\alpha}^2 \varepsilon_{\beta\beta}^2$ is the permittivity corresponding to the wave vector q, p_{qQ} and $p_{q\varepsilon}$ are the elasto-optical constants related to the order parameter Q and the acoustic strain ε_B, and D is a constant that takes into account geometrical and other factors that are independent of frequency ω and temperature T. The quantity χ_{ij} can be found from the matrix equation

$$\begin{Vmatrix} \chi_Q^{-1} & a \\ a & \chi_\varepsilon^{-1} \end{Vmatrix} \cdot \begin{Vmatrix} \chi_{QQ} & \chi_{Q\varepsilon} \\ \chi_{\varepsilon Q} & \chi_{\varepsilon\varepsilon} \end{Vmatrix} = \begin{Vmatrix} 1 & 0 \\ 0 & 1 \end{Vmatrix}, \tag{5.45}$$

while the susceptibilities for each mode in the absence of interaction ($a = 0$) are as follows:

$$\chi_Q^{-1} = m^*(\omega_0^2 - \omega^2 - i\omega\Gamma), \quad \chi_\varepsilon^{-1} = \frac{\rho}{q^2}(\omega_0^2 - \omega^2 - i\omega\Gamma). \tag{5.46}$$

Assuming that for the acoustic soft mode $\Gamma \gg \gamma \simeq 0$ and $\omega \ll \omega_0$, we obtain

$$\begin{aligned} \frac{1}{m\omega}\chi''_{QQ} &= \frac{\Gamma}{\left[\omega_0^2 - \dfrac{a}{m^*}\beta(\omega)\right]^2 + [\Gamma\omega]^2}, \\ \frac{1}{m\omega}\chi''_{\varepsilon\varepsilon} &= \frac{\Gamma\beta^2(\omega)}{\left[\omega_0^2 - \dfrac{a}{m^*}\beta(\omega)\right]^2 + [\Gamma\omega]^2}, \\ \frac{1}{m\omega}\chi''_{Q\varepsilon} &= \frac{\Gamma\beta(\omega)}{\left[\omega_0^2 - \dfrac{a}{m^*}\beta(\omega)\right]^2 + [\Gamma\omega]^2}, \end{aligned} \tag{5.47}$$

where

$$\beta(\omega) = \frac{aq^2}{\rho}(\omega_A^2 - \omega^2)^{-1}.$$

In this case, expression (5.44) can be rewritten in the form

$$I_{HH}(\omega) = D'\varepsilon_q^4 T \frac{\left[p_{q\varepsilon} + p_{qQ}\dfrac{1}{\beta(\omega)}\right]^2}{\left[\dfrac{\omega_0^2}{\beta(\omega)} - \dfrac{a}{m^*}\right]^2 + \left[\dfrac{\Gamma\omega}{\beta(\omega)}\right]^2}\ , \tag{5.48}$$

which coincides with the corresponding expression obtained in [78].

The intensity of light scattering by the soft acoustic mode has a maximum at the resonance frequency ω_R, which is determined from the condition of equality to zero of the first term in square brackets in the denominator of (5.48). In this case, the following relationships hold:

$$\omega_R^2 = \omega_A^2 - \frac{a^2q^2}{\rho m^*\omega_0^2}, \quad \beta(\omega_R) = \frac{m^*\omega_0^2}{a}\ , \quad \text{and}$$

$$I_{HH}^R(\omega_R) = D'T\varepsilon_q^4 \frac{[p_{q\varepsilon}\beta(\omega_R) + p_{qQ}]^2}{\Gamma^2\omega_R^2}\ .$$

Assuming a line shape close to the Lorentz one with width $\Delta = \Gamma/\beta^2(\omega)$, we obtain for the integrated intensity I_{HH} measured in the experiment

$$I_{HH} = I_{HH}^R\Delta = D''T\varepsilon_q^4 \frac{\left[p_{q\varepsilon} + \dfrac{p_{qQ}}{\beta(\omega_R)}\right]^2}{\omega_R^2}\ . \tag{5.49}$$

To analyze the experimental data we use the so-called "reduced" intensity J_{HH} [76], in which the factors T and $\varepsilon_q^3 = n^6(T)$ are excluded. These factors are quite smooth in the transition region [53]. Since the flux of scattered light is considered outside the crystal, we use ε_q^3 instead of ε_q^4. We have

$$J_{HH} = \frac{I_{HH}}{Tn^6(T)} = D''\frac{|P|^2}{C_c}\ . \tag{5.50}$$

According to [29] the value of P in (5.50) is

$$P = \left|p_{q\varepsilon} + \frac{\Delta C}{a}p_{qQ}\right| = \begin{cases} p_{q\varepsilon} + \dfrac{a}{A}\cdot\dfrac{p_{qQ}}{T - T_0} & \text{with} \quad T \geq T_c, \\ p_{q\varepsilon} + \dfrac{a}{A}\cdot\dfrac{1-x}{2}\cdot\dfrac{p_{qQ}}{T_c(3-x) - T_0(1-x) - 2T} & \text{with} \quad T < T_c. \end{cases}$$

In Fig. 31, the observed temperature dependence of the intensity of light scattering by the soft acoustic mode is represented. Figure 32 illustrates the temperature variation of the reduced intensity of light scattering by the soft acoustic mode normalized to the absorption coefficient (see Fig. 22).

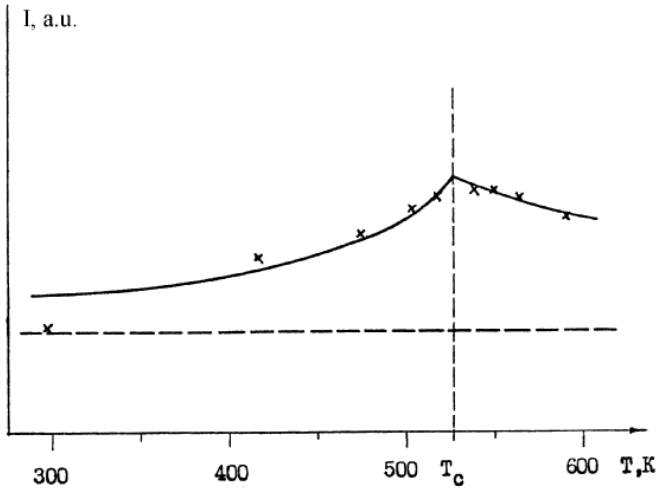

Fig. 31. Temperature dependence of the observed intensity of light scattering by the soft acoustic mode in bismuth vanadate.

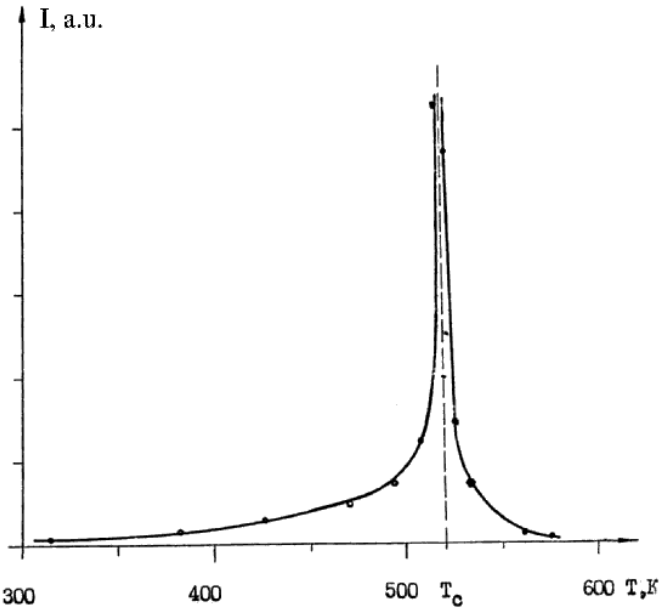

Fig. 32. Temperature dependence of the reduced intensity of light scattering by the soft acoustic mode in bismuth vanadate normalized to the absorption coefficient.

6. Conclusions

The temperature dependences of all components (13 coefficients) of the elastic modulus matrix of bismuth vanadate within the temperature range 300–600 K were obtained for the first time in this paper using the Brillouin scattering technique. It was shown that in the Raman spectra of bismuth vanadate the high-Q soft mode of symmetry A_g (with $T < T_c$) and symmetry B_g (with $T > T_c$) was observed when heating this crystal from room temperature to the phase transition point ($T_c = 522$ K). The soft acoustic mode was observed in the Brillouin scattering spectra close to T_c. The effects of strong coupling of acoustic and optical modes of a ferroelastic $BiVO_4$ crystal were studied by the Brillouin and Raman scattering techniques. The elastic anomalies in the paraelastic phase of bismuth vanadate when approaching T_c were shown to be due to the coupling of the acoustic modes of the crystal with the soft optical mode of symmetry B_g and can be described within the framework of Landau theory with consideration for the interaction terms linear and quadratic in Q. It was found that the strong coupling between the optical and acoustic modes of the same symmetry results in the "repulsion" of their frequencies. It was shown that the mode coupling should result in the renormalization of the phase-transition parameters (increase in T_c and variation of the Curie-Weiss constant).

Experimental studies of the temperature dependences of the components of the spontaneous strain tensor of a single-domain bismuth vanadate crystal were carried out. It was shown that the temperature dependences of the spontaneous strains resulted from their linear (for the B_g strains) and quadratic (for the A_g strains) relation to the order parameter and can be described within the framework of the thermodynamic Landau theory in the temperature range $(T - T_c)/T_c < 0.1$. The temperature dependences of the principal refractive indexes were studied. These dependences were shown to be due to the elasto-optical effect. In this case, the contributions of the primary (of symmetry B_g) and secondary (of symmetry A_g) strains in the paraelastic phase are comparable.

The temperature dependences of the domain-structure parameters of bismuth vanadate were determined experimentally for the first time. The existence of four types of domains differing in the sign of the components of the distortion tensor was shown. Their compatibility is provided by the reciprocal rotation of domains of different types. The temperature dependence of the domain-structure parameters was shown to be due to the temperature dependence of the spontaneous strain.

A technique for determining the components of both the symmetric and antisymmetric parts of the distortion tensor of the polydomain crystal was proposed. This technique is based on the variation in the angles between the wedging out areas of the neighboring domains at the crystal surface. This allowed us to study the temperature dependence of the strain in domains of various type and to verify experimentally the twinning mechanism in $BiVO_4$.

The temperature dependence of the intensity of Brillouin scattering by the soft acoustic mode in $BiVO_4$ in the phase-transition region was studied. A drastic increase in the intensity of Brillouin scattering was observed close to the transition point (Brillouin opalescence). This is explained by the anomaly of the critical elastic modulus and the variation in the elasto-optical constants.

The results obtained on the possibility of variation in the phase-transition temperature when the vibrational spectrum is modified because of introduction of additional vibrational degrees of freedom or comminution of the macroscopic sample with formation of the ordered superdispersed structure have a common origin. These results can be used to increase the phase-transition temperature in ferroelastics, ferroelectrics, and superconductors.

Acknowledgements

This work was supported by the Russian Foundation for Basic Research (Grants No. 04-02-16237 and 02-02-16221).

References

1. V. L. Ginzburg, *Dokl. Akad. Nauk SSSR*, **105**, 240 (1955).
2. V. L. Ginzburg and A. P. Levanyuk, *Zh. Éksp. Teor. Fiz.*, **39**, 192 (1960).
3. V. L. Ginzburg, *Usp. Fiz. Nauk*, **77**, 621 (1962).
4. W. Cochran, *Adv. Phys.*, **9**, 387 (1960).
5. A. S. Sonin and B. A. Strukov, *Introduction to Ferroelectricity* [in Russian], Vysshaya Shkola, Moscow (1970).
6. R. A. Cowley, *Phys. Rev.* B, **13**, 4877 (1976).
7. S. Aubry and R. Pick, *J. de Phys.*, **32**, 657 (1971).
8. V. S. Gorelik, "Idealized models of crystal lattices and spectra of real crystals," in: M. M. Sushchinsky (Ed.), *Inelastic Light Scattering in Crystals*, *Proceedings of the Lebedev Physical Institute* [in Russian], Nauka, Moscow (1987), Vol. 180, p. 87.
9. M. M. Sushchinsky, "Raman scattering on phase transitions in crystals," in: M. M. Sushchinsky (Ed.), *Raman Scattering and Lattice Dynamics*, *Proceedings of the Lebedev Physical Institute* [in Russian], Nauka, Moscow (1982), Vol. 132, p. 3.
10. V. S. Gorelik, "Study of bound and continual vibrational states in dielectric crystals by the Raman scattering technique," in: M. M. Sushchinsky (Ed.), *Raman Scattering and Lattice Dynamics*, *Proceedings of the Lebedev Physical Institute* [in Russian], Nauka, Moscow (1982), Vol. 132, p. 16.
11. V. L. Ginzburg, "Several remarks on ferroelectricity, soft modes, and related issues," in: M. M. Sushchinsky (Ed.), *Inelastic Light Scattering in Crystals*, *Proceedings of the Lebedev Physical Institute* [in Russian], Nauka, Moscow (1987), Vol. 180, p. 3.
12. B. A. Strukov, *Ferroelectricity* [in Russian], Nauka, Moscow (1979).
13. B. A. Strukov and A. P. Levanyuk, *Physical Fundamentals of the Ferroelectric Phenomena in Crystals* [in Russian], Nauka, Moscow (1995).
14. E. M. Brody and H. Z. Cummins, *Phys. Rev. Lett.*, **21**, 1263 (1968).
15. E. M. Brody and H. Z. Cummins, *Phys. Rev. Lett.*, **23**, 1039 (1969).
16. B. A. Strukov, A. V. Davtyan, K. A. Minaeva, and A. A. Gornaev, *Izv. Akad. Nauk SSSR, Ser. Fiz.*, **47**, 611 (1983).
17. B. A. Strukov and K. A. Minaeva, *Prib. Tekh. Éksp.*, No. 6, 157 (1986).
18. V. G. Martynov, K. S. Aleksandrov, and A. T. Anistratov, *Fiz. Tverd. Tela*, **15**, 2922 (1973).
19. U. M. Madvaliev, Yu. M. Sandler, V. I. Serikov, and O. Yu. Serdobol'skaya, *Fiz. Tverd. Tela*, **19**, 900 (1977).
20. L. P. Avakyants and D. F. Kiselev, "Changes in Elastooptic Constants of Uniaxial Ferroelectric Crystals with Second-Order Phase Transitions," *VINITI*, No. 414-78 (1978).
21. E. F. Dudnik, V. V. Gene, S. V. Akimov, and S. A. Kreicherek, *Fiz. Tverd. Tela*, **16**, 2723 (1974).
22. J. D. Bierlein and A. W. Sleight, *Sol. State Commun.*, **16**, 69 (1975).
23. K. Aizu, *J. Phys. Soc. Jpn.*, **28**, 706 (1970).
24. A. Pinczuk, G. Burns, and F. H. Dacol, *Sol. State. Commun.*, **24**, 163 (1977).

25. A. Pinczuk, B. Welber, and F. H. Dacol, *Sol. State. Commun.*, **29**, 515 (1979).
26. W. I. David, A. M. Glayzer, and A. W. Hewat, *Phase Transition*, **1**, 155 (1979).
27. B. Gu, M. Copic, and H. Z. Cummins, *Phys. Rev.* B, **24**, 4098 (1981).
28. M. Cho, T. Yagi, T. Fujii, et al., *J. Phys. Soc. Jpn.*, **51**, 2914 (1982).
29. L. P. Avakyants, E. F. Dudnik, D. F. Kiselev, and I. E. Mnushkina, *Fiz. Tverd. Tela*, **25**, 1910 (1983).
30. H. Tokumoto and H. Unoki, *Phys. Rev.* B, **27**, 3748 (1983).
31. B. Y. Gu, H. Z. Cummins, S. L. Qiu, and M. Copic, *Ferroelectrics*, **52**, 45 (1983).
32. J. G. Wood and A. M. Glayzer, *J. Appl. Cryst.*, **13**, 217 (1980).
33. W. I. F. David, *J. Phys. C: Sol. St. Phys.*, **16**, 5093 (1983).
34. W. I. F. David, *J. Phys. C: Sol. St. Phys.*, **16**, 5119 (1983).
35. W. I. F. David and J. G. Wood, *J. Phys. C: Sol. St. Phys.*, **16**, 5127 (1983).
36. J. F. Nye, *Physical Properties of Crystals*, Clarendon Press, Oxford (1964).
37. W. I. F. David and J. G. Wood, *J. Phys. C: Solid State Phys.*, **16**, 5149 (1983).
38. K. J. Fousek and V. Janovec, *J. Appl. Phys.*, **40**, 135 (1969).
39. J. Sapriel, *Phys. Rev.* B, **12**, 5128 (1975).
40. Y. Ishibashi, *J. Phys. Soc. Jpn.*, **47**, 1857 (1979).
41. C. Manolikas and S. Amelinckx, *Phys. St. Sol.*, **A60**, 167 (1980).
42. L. S. Wainer, R. F. Baggio, H. L. Dussel, and H. A. Benyacar, *Ferroelectrics*, **31**, 121 (1981).
43. I. E. Mnushkina and E. F. Dudnik, *Kristallografiya*, **27**, 805 (1982).
44. S. V. Akimov, I. E. Mnushkina, and E. F. Dudnik, *Zh. Tekh. Fiz.*, **52**, 784 (1982).
45. E. F. Dudnik, V. V. Gene, and I. E. Mnushkina, *Izv. Akad. Nauk SSSR, Ser. Fiz.*, **43**, 1723 (1979).
46. E. F. Dudnik, I. E. Mnushkina, and V. V. Gene, *Fiz. Tverd. Tela*, **23**, 576 (1981).
47. D. L. Wood and J. W. Fleming, *Rev. Sci. Instr.*, **53**, 43 (1982).
48. L. P. Avakyants, D. F. Kiselev, and A. V. Chervyakov, *Izv. Akad. Nauk SSSR, Ser. Fiz.*, **48**, 1107 (1984).
49. A. M. Sleight, H.-Y. Cun, A. Ferreti, and D. E. Coh, *Mater. Res. Bull.*, **14**, 1571 (1979).
50. L. P. Avakyants, D. F. Kiselev, and A. V. Chervyakov, *Fiz. Tverd. Tela*, **27**, 231 (1985).
51. L. P. Avakyants, D. F. Kiselev, and A. V. Chervyakov, "Determination of the spontaneous strain in polydomain ferroelectric crystals" [in Russian], Preprint of the Physical Faculty of Moscow State University, No. 11/1988, Moscow (1988).
52. L. P. Avakyants, D. F. Kiselev, and A. V. Chervyakov, "Temperature dependence of the components of the spontaneous strain tensor of polydomain $BiVO_4$ ferroelastic crystals" [in Russian], in: *Book of Abstracts of the VI All-Russian Workshop "Ferroelastics (Properties and Applications),"* Dnepropetrovsk (1988), p. 77.
53. L. P. Avakyants, D. F. Kiselev, and A. V. Chervyakov, *Fiz. Tverd. Tela*, **25**, 2782 (1983).
54. G. N. Zhizhin, B. N. Mavrin, and V. F. Shabanov, *Optical Vibrational Spectra of Crystals* [in Russian], Nauka, Moscow (1984).
55. H. Poulet and J. P. Mathieu, *Spectres de Vibration et Symetrie des Cristaux*, Gordon & Breach, Paris (1970).
56. G. B. Bokii, *Crystal Chemistry* [in Russian], Nauka, Moscow (1971).
57. K. Nakamoto, *Infrared Spectra of Inorganic and Coordination Compounds*, Wiley, New York (1963).
58. L. P. Avakyants, I. A. Kitov, and A. V. Chervyakov, *Prib. Tekh. Éksp.*, No. 2, 145 (1988).
59. L. D. Landau and E. M. Lifshitz, *Theory of Elasticity*, 3rd English ed., Pergamon Press, Oxford

(1986).
60. A. M. Kosevich, *Fundamentals of Crystal Lattice Mechanics* [in Russian], Nauka, Moscow (1972).
61. F. I. Fedorov, *Theory of Elastic Waves in Crystals*, Plenum Press, New York (1968).
62. Yu. I. Sirotin and M. P. Shaskol'skaya, *Fundamentals of Crystal Physics* [in Russian], Nauka, Moscow (1979).
63. V. E. Lyamov, *Polarization Effects and Anisotropy of Interaction of Acoustic Waves in Crystals* [in Russian], Moscow State University Publishers, Moscow (1983).
64. D. J. Hudson, *Lectures on Elementary Statistics and Probability*, CERN, Geneva (1963).
65. C. R. Rao, *Linear Statistical Inference and Its Applications*, 2nd ed., Wiley, New York (1973).
66. A. A. Afifi and S. P. Azen, *Statistical Analysis*, Academic Press, New York–San-Francisco–London (1979).
67. N. Draper and H. Smith, *Applied Regression Analysis*, Wiley, New York (1966).
68. N. M. Kalitkin, *Numerical Methods* [in Russian], Nauka, Moscow (1978).
69. L. P. Avakyants, D. F. Kiselev, and A. V. Chervyakov, *Kristallografiya*, **30**, 1021 (1985).
70. L. P. Avakyants, D. F. Kiselev, and A. V. Chervyakov, "Intensity of light scattering by soft optical and acoustic modes in the region of the ferroelastic phase transition in $BiVO_4$" [in Russian], in: *Book of Abstracts of the VI All-Russian Workshop "Ferroelastics (Properties and Applications),"* Dnepropetrovsk (1988), p. 78.
71. L. P. Avakyants, I. A. Kitov, and A. V. Chervyakov, "Automated set-up for studies of Mandelstam–Brillouin scattering on the basis of the "Elektronika-60" computer" [in Russian], in: *Book of Abstracts of the XX All-Russian Spectroscopy Congress*, Kiev (1988), part 2, p. 77.
72. L. P. Avakyants, S. V. Akimov, A. M. Antonenko, et al., *Fiz. Tverd. Tela*, **24**, 2486 (1982).
73. V. V. Lemanov, S. Kh. Esayan, and Zh. P. Shapel', *Fiz. Tverd. Tela*, **23**, 262 (1981).
74. V. L. Ginzburg, A. P. Levanyuk, and A. A. Sobyanin, *Usp. Fiz. Nauk*, **130**, 615 (1980).
75. D. G. Sannikov, *Fiz. Tverd. Tela*, **4**, 1619 (1962).
76. V. S. Gorelik, "On the anomalies of the spectral intensity of inelastic light scattering near the phase transition point in crystals," in: M. M. Sushchinsky (Ed.), *Inelastic Light Scattering in Crystals*, *Proceedings of the Lebedev Physical Institute* [in Russian], Nauka, Moscow (1987), Vol. 180, p. 180.
77. R. L. Reese, I. J. Fritz, and H. Z. Cummins, *Phys. Rev.* B, **37**, 4165 (1973).
78. D. F. Nelson, P. D. Lazay, and M. Lax, *Phys. Rev.* B, **6**, 3109 (1972).